SAHC

Static Stress Analysis of the Janov Dam
Historic Masonry Gravity Dam

Constantin Groud

Czech Republic | 2023

ADVANCED MASTERS IN STRUCTURAL ANALYSIS
OF MONUMENTS AND HISTORICAL CONSTRUCTIONS

Master's Thesis

Constantin Gourd

Static Stress Analysis of the Janov Dam - Historic Masonry Gravity Dam.

University of Minho

Czech Republic | 2023

CZECH TECHNICAL UNIVERSITY IN PRAGUE
Faculty of Civil Engineering
Thákurova 7, 166 29 Prague 6, Czech Republic

DIPLOMA THESIS ASSIGNMENT FORM

I. PERSONAL AND STUDY DATA

Surname: Gourd Name: Constantin Personal number: 520833

Assigning Department: Department of Hydraulic Structures

Study programme: Civil Engineering

Study branch/spec.: Advanced Masters in Structural Analysis of Monuments and Historical Constructions

II. DIPLOMA THESIS DATA

Diploma Thesis (DT) title: Static Stress Analysis of the Janov Dam - Historic Masonry Gravity Dam

Diploma Thesis title in English: Static Stress Analysis of the Janov Dam - Historic Masonry Gravity Dam

Instructions for writing the thesis:
Based on the general theroy of masonry dam construction, describe the Janov dam and its history.
Carry out a static stress analysis of a dam by building and calibrating numerical model in provide software.
Describe the development of model topology, used constitutive models and solution methods. Analyze the available uplift and displacement measurements for calibration of the model and comment on results from the allowable stress pont of view.

List of recommended literature:
Hydraulic Structures, Novak et. al. ISBN 0-203-96463-2; EM 1110-2-2200 USACE; ICOLD Bulletin no. 155; ATENA

Name of Diploma Thesis Supervisor: Ing. Miroslav Broucek, Ph.D.

DT assignment date: 14.3.2023 DT submission date in IS KOS: 6.7.2023
see the schedule of the current acad. year

DT Supervisor's signature Head of Department's signature

III. ASSIGNMENT RECEIPT

I declare that I am obliged to write the Diploma Thesis on my own, without anyone's assistance, except for provided consultations. The list of references, other sources and consultants' names must be stated in the Diploma Thesis and in referencing I must abide by the CTU methodological manual "How to Write University Final Theses" and the CTU methodological instruction "On the Observation of Ethical Principles in the Preparation of University Final Theses".

Assignment receipt date Student's name

DECLARATION

Name:	Constantin Gourd
Email:	Contantingourd@gmail.com

Title of the Msc Dissertation:	Static Stress Analysis of Janov Dam – Historic Masonry Gravity Dam
Supervisor(s):	Miroslav Brouček
Year:	2023

I hereby declare that all information in this document has been obtained and presented in accordance with academic rules and ethical conduct. I also declare that, as required by these rules and conduct, I have fully cited and referenced all material and results that are not original to this work.

I hereby declare that the MSc Consortium responsible for the Advanced Masters in Structural Analysis of Monuments and Historical Constructions is allowed to store and make available electronically the present MSc Dissertation.

University:	Czech Technical University in Prague
Date:	05/07/2023
Signature:	_____

ACKNOWLEDGEMENTS

First of all, I would like to thank my thesis supervisor, Professor Miroslav Broucek, who has given me constant support throughout this project, on both an engineering and a personal level.

I would like to express my deep gratitude to the staff of CTU University, in particular Professor Petr Kabele, who has accompanied us throughout this experience and supported us during the ordeals that some of my colleagues have gone through.

I would like to thank Safa Joudeh for the help she provided me in creating the 3D model

I'd like to thank the SAHC community for the camaraderie and inspiration that make work like this possible, and which we'll continue to nurture.

Finally, I thank U Minho, CTUV Prague & SAHC master's for the support of the Consortium Scholarship 2023.

ABSTRACT

This thesis studies the effect of hydrostatic and thermal loading on the evolution of static stresses and strains in the Janov gravity dam, using a finite element model (FEM).

The first step is to describe the model development process, such as the generation of the model geometry and materials. The dam and its rock foundation are modeled as macro-elements. The joint between the macro-blocks is represented by a Mohr-Coulomb connection. The geometry is based on a section of the dam (section 5L), taken from the technical report on the Janov dam bedrock. The material properties are based on tests carried out on the dam in 2000-2015, the results of which are referenced in the technical report.

Static and thermal loading analyses were used to study the magnitude and nature of stresses and displacements at critical points in the dam. The results show that the analytical approach mentioned in *LES BARRAGES Du projet à la mise en service, volume 17, 2011* underestimates the magnitude of stresses at the upstream and downstream toes of the dam, compared with the FEM model values. In addition, a non-linear distribution of normal stresses σyy at the dam interface is observed in the case of the non-linear FEM model, unlike the conventional linear model specified in *LES BARRAGES Du projet à la mise en service, volume 17, 2011.*

A comparison with IN-SITU data retrieved from the dam then enables the model to be calibrated. To monitor the structural integrity of the Janov dam, a Huggenberg GL50 - 100 pendulum was installed in its central tower. This system provides real-time data on the deformation of the dam in the horizontal plane. The calibration results show higher masonry material properties for static loading than for thermal loading. This difference is due to the 3D effect which explains the need to reinforce the 2D model for the static analysis.

ABSTRACT

Tato práce se zabývá vlivem hydrostatického a tepelného zatížení na vývoj statických napětí a deformace v gravitační přehradě Janov pomocí modelu konečných prvků (MKP).

Prvním krokem je popis procesu vývoje modelu, jako je generování geometrie modelu a materiálů. Přehrada a její skalní podloží jsou modelovány jako makroelementy. Spoj mezi makrobloky je reprezentován Mohr-Coulombovým spojem. Geometrie vychází z řezu hráze (řez 5L), který byl převzat z geotechnické zprávy o skalním podloží Janovské přehrady. Materiálové vlastnosti vycházejí ze zkoušek provedených na hrázi v letech 2000-2015, na jejichž výsledky je odkazováno v technické zprávě.

Ke studiu velikosti a charakteru napětí a posunů v kritických bodech hráze byly použity statické a tepelné zatěžovací analýzy. Výsledky ukazují, že analytický přístup uvedený v *LES BARRAGES Du projet à la mise en service, volume 17, 2011*. podhodnocuje velikost napětí v patě a špičce hráze ve srovnání s hodnotami modelu FEM. Kromě toho je v případě nelineárního modelu FEM pozorováno nelineární rozložení normálových napětí σyy na rozhraní hráze, na rozdíl od konvenčního lineárního modelu uvedeného v *LES BARRAGES Du projet à la mise en service, volume 17, 2011*.

Porovnání s údaji IN-SITU získanými z přehrady pak umožňuje kalibraci modelu. Pro sledování strukturální integrity janovské přehrady bylo v její centrální věži instalováno kyvadlo Huggenberg GL50 - 100. Kyvadlo bylo umístěno na výšce 1,5 metru. Tento systém poskytuje údaje o deformaci hráze v horizontální rovině v reálném čase. Výsledky kalibrace ukazují vyšší vlastnosti materiálu zdiva pro statické zatížení než pro tepelné zatížení. Tento rozdíl je způsoben 3D efektem, který vysvětluje potřebu posílit 2D model pro statickou analýzu.

ABSTRACT

Cette thèse étudie l'effet des charges hydrostatique et thermique sur l'évolution des contraintes statiques et déformations du barrage-poids de Janov à l'aide d'un modèle éléments finis (FEM).

La première étape consiste à décrire le processus de développement du modèle, notamment la génération de la géométrie et des matériaux du modèle. Le barrage et sa fondation rocheuse sont modélisés comme des macro-éléments. Le joint entre les macro-blocs est représenté par une connexion Mohr-Coulomb. La géométrie est basée sur une section du barrage (section 5L), tirée du rapport géotechnique sur les fondations du barrage de Janov. Les propriétés des matériaux sont basées sur des tests effectués sur le barrage en 2000-2015, dont les résultats sont référencés dans le rapport technique.

Des analyses de charge statique et thermique ont été utilisées pour étudier l'ampleur et la nature des contraintes et des déplacements aux points critiques du barrage. Les résultats montrent que l'approche analytique mentionnée dans *LES BARRAGES Du projet à la mise en service, volume 17, 2011* sous-estime l'ampleur des contraintes au talon et au pied du barrage, par rapport aux valeurs du modèle FEM. En outre, une distribution non linéaire des contraintes verticales σyy à l'interface du barrage est observée dans le cas du modèle FEM non linéaire, contrairement au modèle linéaire conventionnel spécifié dans *LES BARRAGES Du projet à la mise en service, volume 17, 2011*.

Une comparaison avec les données IN-SITU extraites du barrage permet ensuite de calibrer le modèle. Pour surveiller l'intégrité structurelle du barrage de Janov, un pendule Huggenberg GL50 - 100 a été installé dans sa tour centrale. Ce système fournit des données en temps réel sur la déformation du barrage dans le plan horizontal. Les résultats de l'étalonnage montrent que les propriétés des matériaux de maçonnerie sont plus élevées pour la charge statique que pour la charge thermique. Cette différence est due à l'effet 3D, ce qui explique la nécessité de renforcer le modèle 2D pour l'analyse statique.

TABLE OF CONTENTS

LIST OF FIGURES

LIST OF TABLES

1 INTRODUCTION

1.1 CASE STUDY: JANOV DAM

The Janov dam or Mosteckà dam is located at the confluence of the Loupnice and Klinské potok rivers in Hamerská údolí (see figure 1.1.a). Construction began in June 1911 and was completed in December 1913. "At the beginning of the 20th century, water supply capacity was disastrous for the town of Most". The decision was therefore taken to build a reservoir capable of supplying the town and several other villages with drinking water. Today, the reservoir is listed as a cultural monument and is considered the highest masonry dam in the Czech Republic (44,5 m high). The Janov dam is a gravity dam, but as shown in figure 1.1.b, it follows a curved shape between its two shores. This shape is what makes the Janov dam so special, as its imposing form counteracts the push of the water, and its curved shape deflects some of the water pressure towards the support points. The shores play the same role as the load-bearing walls of a building.

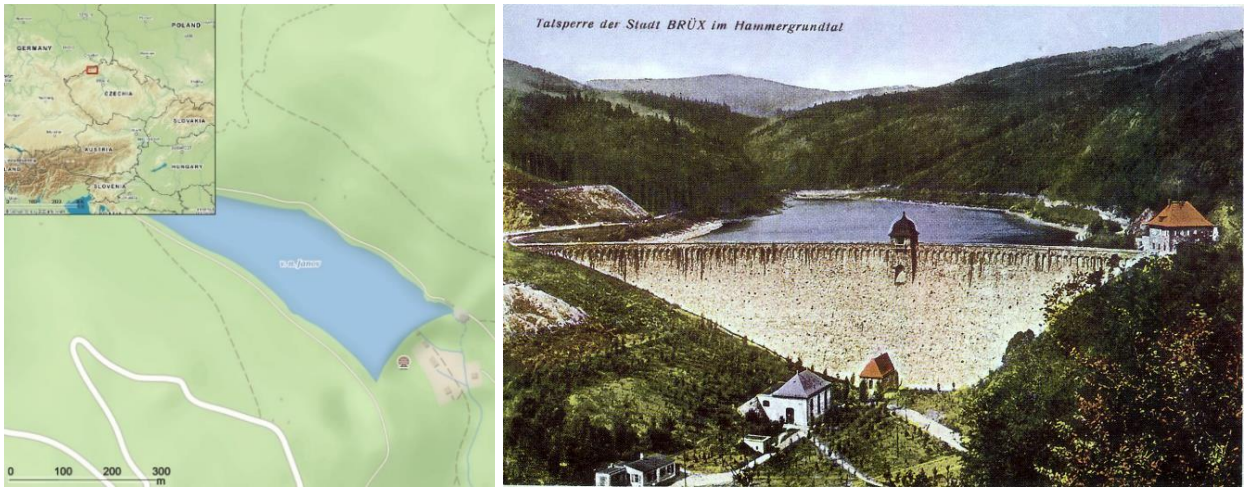

Figure 1.1 - the Loupnice stream valley (a) map localization; (b) Mostecká dam after completion, year 1920, © Panoráma starého Mostecka.

1.2 THESE OUTLINE

This dissertation is divided into 8 chapters. It begins with an introduction, presenting the main aim, objectives and scope of the study, discussing its motivations and context. Chapter 2 deals with the history of the dam, through the stages of planning, construction and repair since the early 20th century. Chapter 3 reviews the theory of gravity dams, their form, applied loads and stresses and displacements.

These theories are then used in Chapters 4, 5 and 6, to develop a finite element model (FEM) of the Janov dam, from its geometric creation to the calibration of its materials.

Chapter 7 deals with the creation of the 3D model of the dam. Finally, Chapter 8 provides the main conclusions of the thesis, followed by some recommendations for the development of the 3D model.

1.3 AIM AND SCOPE

This thesis studies the effect of hydrostatic and thermal loading on the evolution of static stresses and strains in the Janov gravity dam, using a finite element model (FEM).

the main objectives of this study are to describe the model development process, including the generation of the model geometry and materials. Static and thermal loading analyses are then used to study the magnitude and nature of stresses and displacements at critical points in the dam. Finally, a comparison with IN-SITU data recovered from the dam enables the model to be calibrated.

Due to the limited duration of the project, only two-dimensional analyses were carried out.

1.4 MOTIVATION AND CONTEXT

The Janov Dam is a historic 44.5 m-high masonry gravity dam, built between 1911 and 1914, and also a cultural heritage structure of the Czech Republic.

A major rehabilitation project has been carried out in recent years to meet increasing dam safety requirements and improve the dam's behavior in terms of seepage and uplift pressures.

The work is motivated by the assessment of the static behavior of the Janov dam and the creation of a numerical model based on this behavior.

1.5 METHODOLOGY

Figure 1.2 shows the methodology used for this project. The first step is to identify the system. This stage begins with identifying the geometry, from project planning and groundbreaking to repair work. To this end, historical research based on literary sources of the time, photographs and eyewitness accounts was carried out. The results of this research are summarized in the historical review section. The aim is to identify the dam's geometry through its construction process at the time and the renovation works that modified it. This is followed by analytical calculations enabling the nature of the stresses and displacements to be identified theoretically. Then comes the identification of materials and their properties. This part is based on the Eurocodes and on tests previously carried out on the structure.

The second step is the finite element modeling of the previously identified geometry. In the case of the non-linear model, identifying the materials and the laws they follow is of prime importance. Next comes the creation of the model's boundary conditions. The correct generation of the mesh is essential to the study of the model, as a poor mesh can lead to convergence problems and distort the results. The static and thermal loads estimated on the basis of the analytical study are then applied to the model.

The third step is to calibrate the model. This calibration is based on IN-SITU relative displacement datas from a pendulum installed on the dam. This system provides real-time data on the deformation of the dam in the horizontal plane. Calibration is then based on point displacement due to hydrostatic or thermal

loading. Certain parameters of the numerical model are then modified to make the model converge towards the same deformations as the real dam.

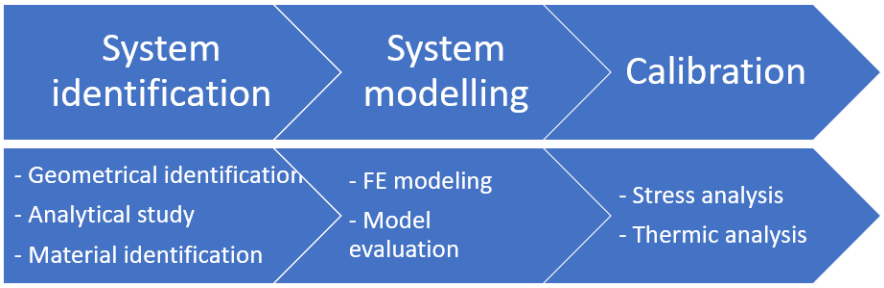

Figure 1.2 - Methodology

2 HISTORICAL SURVEY

2.1 MOST IN THE 20TH CENTURY

At the beginning of the 20th century, the town of Most took its first steps into the era of industrialization. This golden age for the mining industry in the region had catastrophic repercussions for water supply of the population. On the one hand these activities were very water consuming and on the other hand very polluting for the rivers of the region.

In response to this situation, in October 1916 the city council of Most issued a permit for the construction of the Janov dam in the Loupnice stream valley to provide the population with a supply of drinking water.

The choice of location was first of all economic, as the land in Hamerské údolí belonged to the town. It was also practical, because the dam would hold back the spring water that the Loupnice River was carrying into the valley, which caused floods and damage every year.

The decision was made to entrust the supervision of the whole building to the engineer R. Weyrauch, a professor at the University of Stuttgart.

2.2 PREPARATORY WORKS

In the summer of 1911, the municipality of Most called for tenders to determine which company would be responsible for the construction of the dam. This competition was won by the company "Entrepreneurship of valley dams Berndr, Schwarzer a Wurm".

Preparatory work had already begun with the felling and cleaning of the bottom of the future Hamerské údolí reservoir as well as the relocation of the valley road and a new arterial road linking Janov to Mníšek.

The question of transportation of materials in the valley arose. With the exception of one steam locomotive, all engines were electric. For the first time in the Czech Republic, a crane cable was stretched across the valley to enable the import of materials from the road, there were compressors, crushers, mills, elevators and mixers. Four transformers provided power up to 420 kW.

In addition, the construction required a large quantity of massive Gneiss blocks. On June 9, 1911, a "gneiss" quarry was opened on the right side of the valley.

Figure 2.1 - Material transport in the Mostecká valley (a) picture of the wagons, August 20, 1911; (b) picture of the railroad, August 19, 1911; (c) picture of the cable crane tower, March 1912, © Panoráma starého Mostecka.

2.3 THE FOUNDATIONS

The preparation of the foundations began with the clearing, grubbing, stripping and cleaning of the areas on which the dam would be built.

On the advice of Prof. Dr. Laube from Prague, who carried out the geological study, deep trenches were dug in the valley slope and in the valley floor to ensure the necessary safety and stability of the construction.

This was followed, on April 22, 1912, by the pouring of cement mortar to fill the underground voids of the foundation and the cleaning of the surface with pressurized water and steel brushes.

Foundation drainage was also installed, consisting of a network of 50 mm diameter drains spaced 6 to 8 m apart located in the embankment wall approximately 1 m above the foundation joint.

Figure 2.2 - Picture of the foundation joint of the dam, cleaned with pressurized water and steel brushes, 26 April 1912, © Panoráma starého Mostecka.

2.4 THE BUILDING

Due to the narrowness of the valley, the decision was made to curve the plan of the dam, so that it would form a horizontal arch, convex upstream. According to Armand Colin, "a road dam transfers most of the thrust to the banks by arch effects. It is like a single-arch bridge that has been quartered upstream. The stability of this type of structure differs essentially from that of the gravity dam, which results from a certain inequality between the variable water thrust and the immutable weight. Here, on the contrary, the support reactions increase as a direct result of the water pressure. The more it increases, the more strongly it applies the structure against the ground, as in an autoclave closure. No slipping or tumbling is possible, as long as the banks hold firm."

Figure 2.3 - Picture of the ceremonial laying of the foundation stone, 4 May 1912, © Panoráma starého Mostecka.

The Gneiss blocks used inside the dam were chosen and adjusted to create an irregular interlocking structure that would resist water infiltration and internal movements caused by temperature variations between upstream and downstream and, above all, by the deformations of the dam structure that was subject to enormous pressure due to the water it retained.

The lifting of the stones on the dam body is, at first, carried out with the help of the lifting tower installed on the downstream face. Wagons were then used to transport them along the dam body. Then, when the crest became too thin for the rails, a Bleichert cable crane was stretched over the dam.

The cement mortar used (1 volume part of Portland cement, 1 volume part of lime, 6 vol. parts of sand from crushed stone, 10% water) between the rubble stones is a thin layer. It plays mainly the role of bonding between the blocks and of transferring the stresses.

In addition, the upstream face is sealed by a triple layer of cement plaster 3 cm thick.

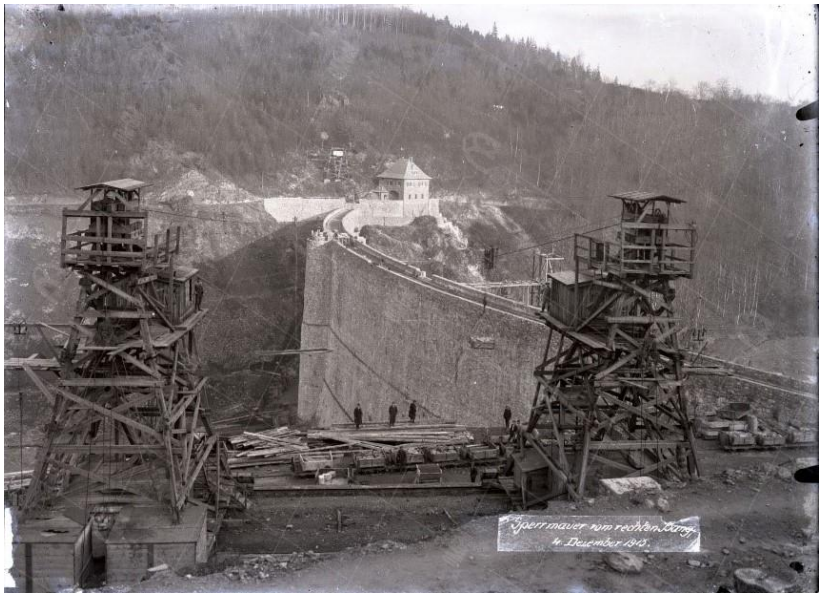

Figure 2.4 - Construction of the dam (a) picture of the dike masonry procedure, July 30, 1913; (b) picture of the upstream face is sealed with a triple coat of 3 cm thick cement plaster, July 12, 1913; (c) picture of the Bleichert rope crane stretched over the dam, October 11, 1913; © Panoráma starého Mostecka.

The dam wall is equipped with a guide (vertical) and foundation (horizontal) drainage system. The vertical drainage is composed of two multi-level water intake system made of 100 mm diameter stoneware pipes at a spacing of 2.0 m. It is located in a semi-circular dry tower building walled to the upstream face of the dam. The foundation drainage consists of a network of drains with a diameter of 50 mm and spacing of 6-8 m placed in the masonry of the dam approximately 1 m above the foundation joint. These drains are connected to collection drains with a diameter of 150 and 200 mm.

In the lower part of the dam, the inspection galleries lead from the main corridor to both sides of the dam, into which the vertical and horizontal drainage systems are led. The right one also served as a sampling pipe for the water treatment plant.

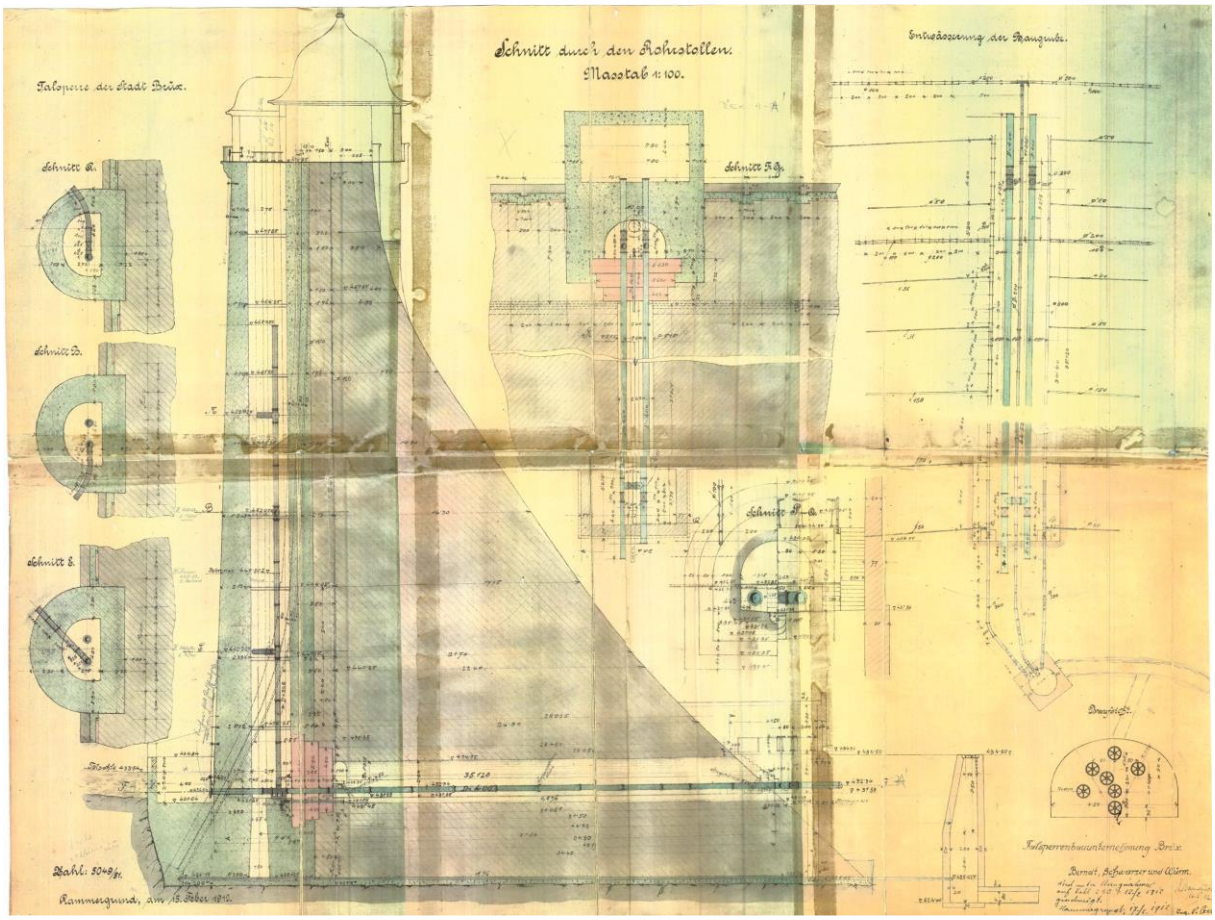

Figure 2.5 - Plan of the original sectional view of the dam, 1911, © Jan Vojtěchovský et al., 2018.

2.5 IN ADDITION TO THE DAM

Figure 2.6 shows the location of the remaining dam systems: (1) At the confluence of the streams, upstream of the reservoir, is a drainage reservoir; (2) the side safety spillway is on the right side of the dam, below (3) the dam operator's house. Two gates are embedded in the spillway for better flood flow management. From the overflow station, water is diverted through a massive rubble cascade downstream of the dam; (4) at the outlet, a penstock leads the water from the dam to the powerhouse to activate a 125 kW Pelton turbine; (5) the water is then stored in an underground drinking water reservoir.

Figure 2.6 - location of the additional buildings

2.6 REPAIR WORK

In early March 1914, when the reservoir was filled for the first time, and the water depth was about 20m, the seepage on the left bank of the dam increased significantly (≈ 133 l/s). The defects were due to subsurface cracks in the left bank connections.

Although the most significant leaks were sealed soon after the dam was built, the subsurface below the dam was not systematically sealed, but only locally. Other local sealing works were carried out in the 1950s and 1970. It can be said that only those places where seepage was visibly rising to the surface were sealed.

Figure 2.7 - First sealing work (a) Seepage in the left bank impoundment appeared soon after the first filling of the reservoir, March 25, 1914; (b) Additional sealing work in the left slope, June 1914, © Panoráma starého Mostecka.

Therefore, the general repair and reconstruction of the dam was started in 2003, which solved this problem once and for all. In two stages, an injection tunnel was dug directly under the dam and the entire subsoil was injected from this tunnel. This was completed in 2013.

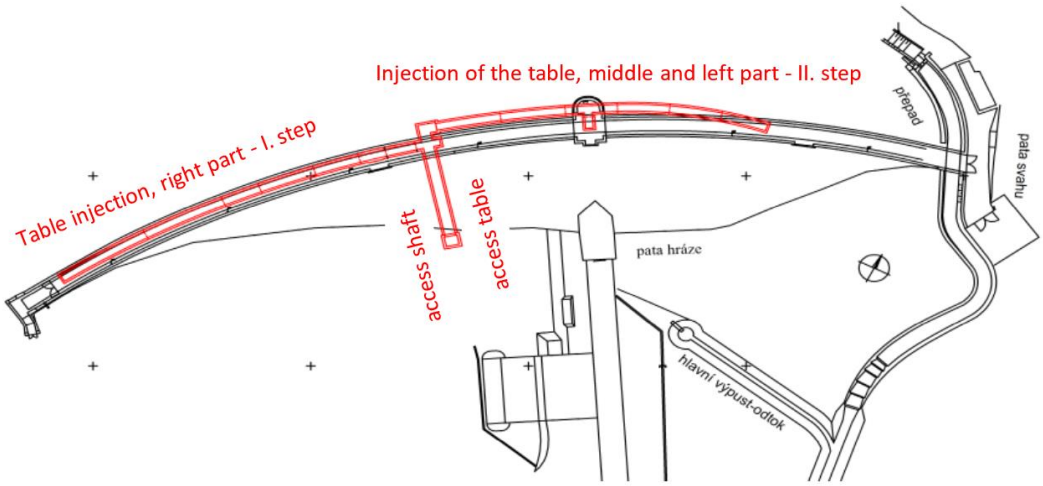

Figure 2.8 - Scheme of the newly built underground facilities at VD Janov, © Jan Vojtěchovský et al., 2018.

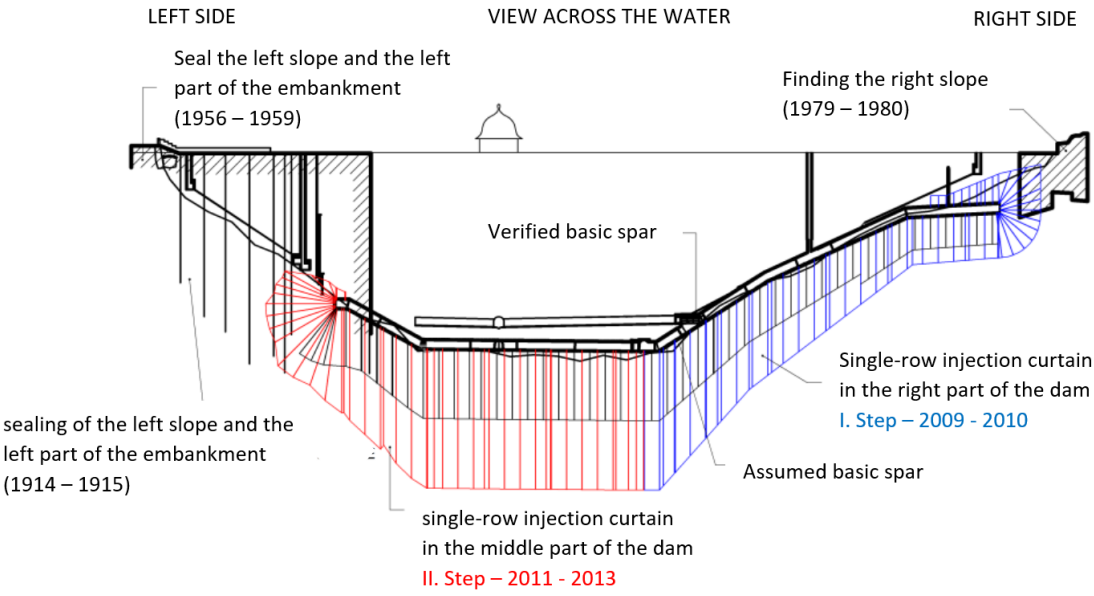

Figure 2.9 - Longitudinal section of the dam, scheme of injection works, view across the water, © Jan Vojtěchovský et al., 2018.

3 ANALYTICAL CALCULATION

A first two-dimensional analytical analysis is carried out on this dam which will then make it possible to verify the stresses applied to the model. During its operation, the dam will be subjected to loads (actions) which will lead to deformations and stresses. These loads entering into the verification calculations of the dams can be distributed according to their mode of application in the three categories: (i) the permanent loads are always present. It is possible however that they appear over time and that they remain without undergoing modifications; (ii) variable loads vary according to operating conditions, others depend on natural conditions; (iii) exceptional charges generally arise following sometimes violent natural events, the effects of which may be sudden or of limited duration.

The table 3.1 presents the different load cases considered for our modelling.

Permanent loads	Variable loads	Extraordinary loads
- gravity load - Earth pressure	- water pressure - Sediment pressure - Uplift pressure - Dam temperature	Ø

Table 3.1 – Loads taken into account for the verification of the dam.

3.1 GENERAL SHAPE

The whole of the study is placed in a local reference point where the point of origin (point 0) is on the interface between the dam-rock and is placed at a height of 442,36 m asl and upstream toe.

For the analytical calculation, the shape of the section is simplified. As presented in figure 3.1, the section is considered massive and solid with a triangular profile. The dam has a height *Hf* of 51,5 m and an upstream side water level *ham* of 49,24 m, a base width *b* of 50,98 m and a crest width *dc* of 7,03 m. The shape of the upstream facing is approximated linearly by a line of inclination φ_1 of 11,2°. The downstream facing is approximated linearly by a straight line with an inclination φ_2 of 32,9°. This geometry allows it to resist by its own weight to overturning and sliding under the action of external forces. The leakage water level is considered zero on the downstream side of the dam.

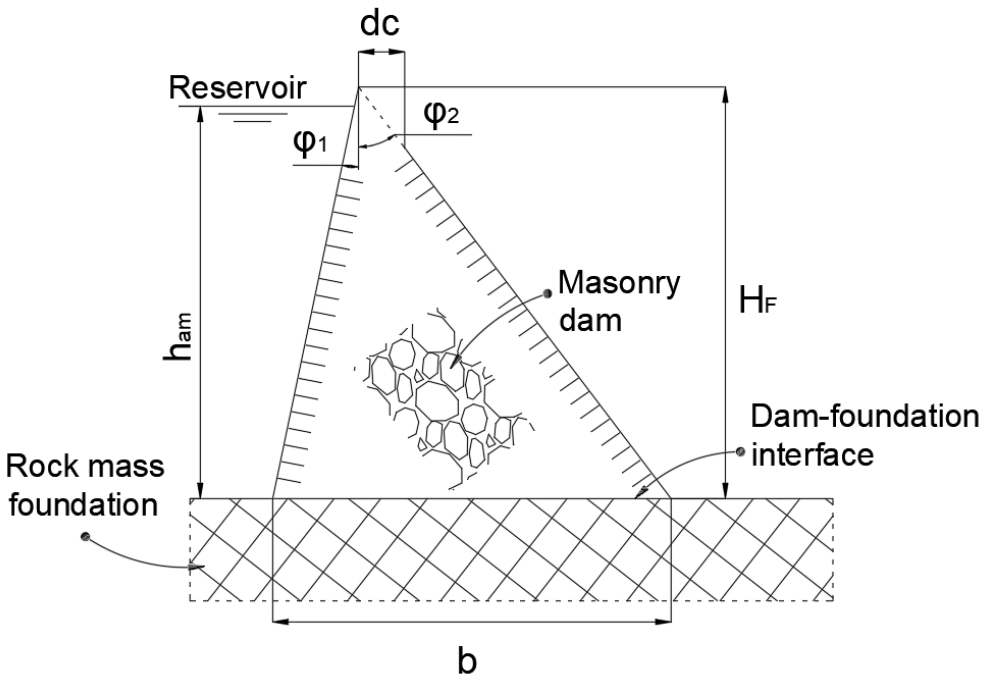

Figure 3.1 - Profile type of the weight dam used for the analytical calculation.

3.2 ACTIONS AND SOLICITATIONS

Description of permanent loads

The dam is subjected to two permanent loads:

The first is self-weight, which is especially of interest in the case of gravity dams. The inner part of the dam is made of rubble masonry and the outer part is covered with a thickness of 0,6 m of Ashlar, the Italian code gives us the following values:

$$\gamma_{rm} = 1{,}9E-2\ MN/m^3 \quad ; \quad \gamma_{ash} = 2{,}2E-2\ MN/m^3 \qquad equation\ 1$$

The second is Earth pressure, which is the action of the embankment downstream on the dam. Here, we take into account a pressure of the earth at rest, it is exerted perpendicularly to the downstream wall of the dam at a height of 8,82 m and is given by the following relationship:

$$F_{TH} = \frac{1}{2}\,\Upsilon_T {h_t}^2\,K_0 = \frac{1}{2}\,\Upsilon_t {h_t}^2\,\frac{\nu}{1-\nu} = 0{,}72\ MN/m \qquad equation\ 2$$

With Υ_T= bulk density and ν= Poisson's ratio of the rock

Description of variable loads

The dam is subjected to three variable loads:

The first is the push of water, which exerts a force perpendicular to the surface of the facing of the dam. Water Density ρ_E is equal to 997 kg/m3. For the calculation, the highest lake level (h_{am}) is chosen in relation to the type of load combination. The values of the various push which act at the center of gravity of their representative surface are as follows:

$$E_{am-h} = \frac{1}{2}\,\rho_E\, g\, {h_{am}}^2 = 12{,}1\ MN\ /\ m \qquad (horizontal\ push\ in\ upstream)\ \ equation\ 3$$

$$E_{am-v} = \frac{1}{2}\,\rho_E\, g\, m_1\, {h_{am}}^2 = 2{,}5\ MN\ /\ m \qquad (vertical\ push\ in\ upstream)\ \ equation\ 4$$

With m_1 = basic width; this value depends on the facing angle $m_1 = tg\ \varphi_1$

The second is the push of the sediments, sediments can accumulate at the upstream toe of a dam and reach a significant thickness, or even sometimes be practically equivalent to the height of the structure. In this case, the height is estimated at 10,4 m and its bulk density at 10,5 kN/m3. These sediments cause a horizontal push on the upstream face which is added to the hydrostatic push and is expressed as:

$$F_{sed} = \frac{1}{2}\,\Upsilon_{sed} {h_{sed}}^2\, K = \ 0{,}42\ MN\ /\ m \qquad equation\ 5$$

With K= earth pressure coefficient; expressed at rest in this situation $K = 1 - \sin \Phi$ and Φ= angle of internal friction estimated at 40°.

The last is the uplift pressure, it exerts an interstitial pressure in the foundation, along concreting stops and sporadic cracks, but also inside the masonry which is porous. A two-part uplift pressure distribution based on the model of the German standard (DIN 19700) is accepted.

To take into account the effect of the grout curtain and the drains, a rectangular distribution allowed at 100% of the hydrostatic pressure is allowed upstream up to the grout curtain. The uplift pressure is then 60% of the hydrostatic pressure. The relationships are as follows:

$$S_{am} = h_{am}\,\rho_E\, g\, d = 4{,}03\ MN\ /\ m \qquad (uplift\ in\ upstream)\ \ equation\ 6$$

$$S_{av} = \frac{1}{2}\,0{,}6\, h_{am}\,\rho_E\, g\,(b-d) = \ 6{,}17\ MN\ /\ m \qquad (uplift\ in\ downstream)\ \ equation\ 7$$

With d= distance between the upstream toe of the dam and the drain.

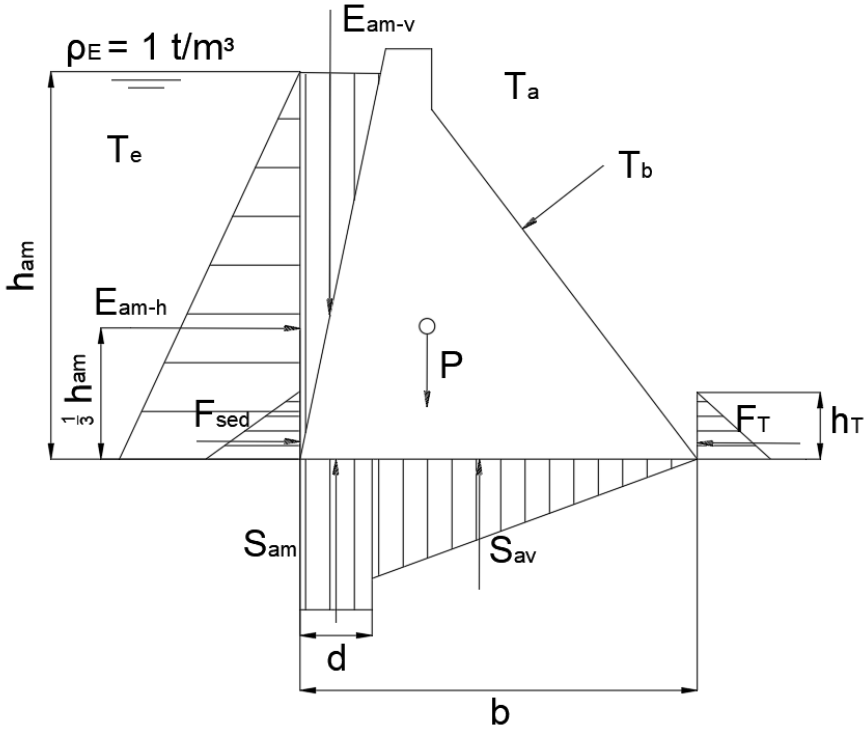

Figure 3.2 - Distribution of forces and actions to be considered. Legend: P= gravity load; E_{am-h}= horizontal push of the upstream water; E_{am-v}= vertical push of the upstream water; F_T= earth pressure; F_{sed}= sediment pressure; S= uplift; T= thermal effect; T_b= dam body temperature; T_a= air temperature; T_e= water temperature; H_F= Height of dam on foundation; h_{am}= Hydrostatic head upstream; h_T= Height of the embankment downstream.

3.3 DISTRIBUTION OF STRESS UNDER THE DAM

Navier's hypothesis assumes that normal stresses vary linearly along a horizontal section. The stress distribution which takes the form of a trapezoid or triangle.

Under the effect of the gravity load, the pressure of the earth, the pressure of the water, the pressure of the sediments, and the uplift pressure, the conditions of balance of the forces on the section lead to the following constraints:

$$\sigma_{y,am} = g\ \rho_B\ H_F\ - g\ \rho_E\ h_{am}\ (m^{-2} + k) - g\ \rho_{sed}\ h_{sed}\ m^{-2} = 1{,}00E-1\ MN\ /\ m^2 \qquad equation\ 8$$

$$\sigma_{y,av} = g\ \ \rho_E\ h_{am}\ m^{-2} + g\ \rho_{sed}\ h_{sed}\ m^{-2} = -5{,}90E-1\ MN\ /\ m^2 \qquad equation\ 9$$

With k= estimated uplift coefficient equal to 1; m= base width, this value depends on the facing angle $m = tg\ \varphi$

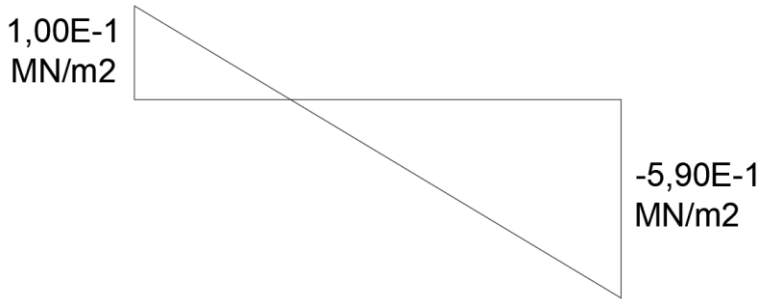

Figure 3.3 - Distribution of normal stresses in the horizontal section.

4 FE MODEL FOR THE CASE STUDY

The objective of this part is to perform an analysis of the static stresses of the Janov dam by building and calibrating a numerical model. (i) The first step is the description of the model development steps such as geometry generation; the materials making up the model; applied static loads; heat flows. (ii) A static stress analysis by finite elements is then carried out in order to analyze the displacement of the model. (iii) A comparison with the in-situ data collected on the dam should then allow the calibration of the model.

The digital model of the masonry dam and its rock foundations are modeled using the finite element method (FEM). The advantage of this method is to be able to model structures of complex geometry, as well as the foundation, taking into account its geomechanical particularities. The ATENA 2D software is used, it is a finite element code developed for the nonlinear analysis of reinforced concrete structures.

4.1 DAM GEOMETRY

Figure 4.1 presents the attributes of the 2D section modeled on ATENA 2D for the present study. This section follows the outline of the diagram of the analytical part while being more in line with section 5L based on the actual attributes of the dam. Section 5L comes from the technical report carried out on the rock mass of the Janov dam in 2010-2015.

In order to monitor the structural integrity of the Janov dam, a Huggenberg GL50–100 pendulum was installed in the central tower. The IN-SITU data of this installation will then be essential for us for the calibration part. The 2D model produced is a set of three monoblocs: (i) the body of the dam is mainly composed of rubble masonry covered with a thickness of 0,6 m of ashlar. From the outside, it has a height *Hf* of 51,5 m and an upstream side water level *ham* of 49,24 m, a base width *b* of 50,98 m and a crest width *dc* of 7,03 m. The shapes of the upstream and downstream facings are now arcs of circles *R1* and *R2*, with respective radii of 116 m and 226m; (ii) inside there is a main gallery and a secondary gallery; (iii) the dam is founded on a base of rock mass with a width of 150 m and a depth of 50 m (model dimension). These dimensions are recommended in order to best approximate the behavior of the semi-infinite medium

constituted by the foundation. The leakage water level is considered zero on the downstream side of the dam.

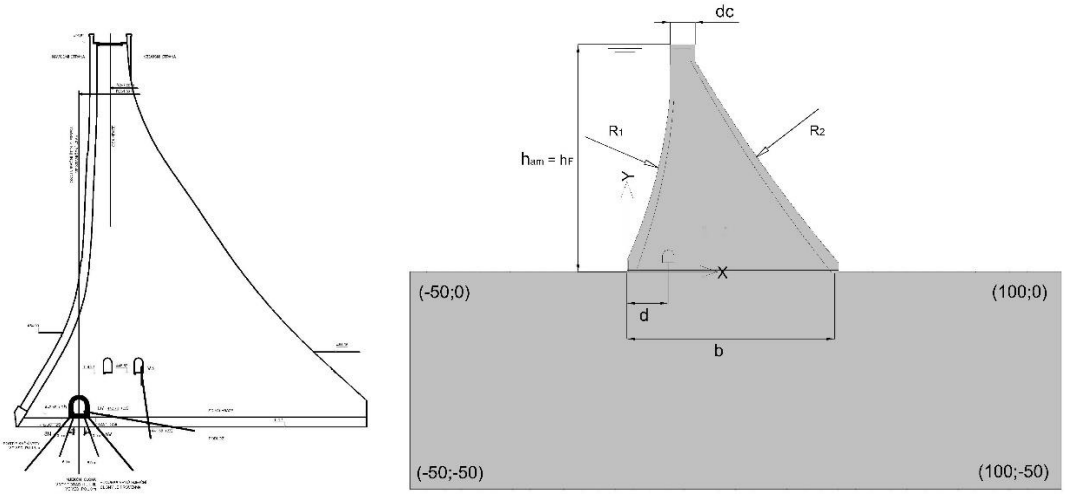

Figure 4.1 - Geometries of the dam and its foundations considered for the analysis: (a) section 5L © Technical report; (b) section modelized on ATENA.

4.2 MESH

The meshes applied to the model are presented in the figure 4.2. Triangular linear elements were used for masonry and rock of coarse sizes between 1 and 3 meters to save calculation time. Due to the static loads applied to the model, stress concentrations are expected at the dam-rock interface and mainly at the upstream and downstream toes of the dam. This is why “By size and Radius” type mesh refinements have been applied to these points with an element size at joints 1 and 3 between 0,5 and 0,6 m.

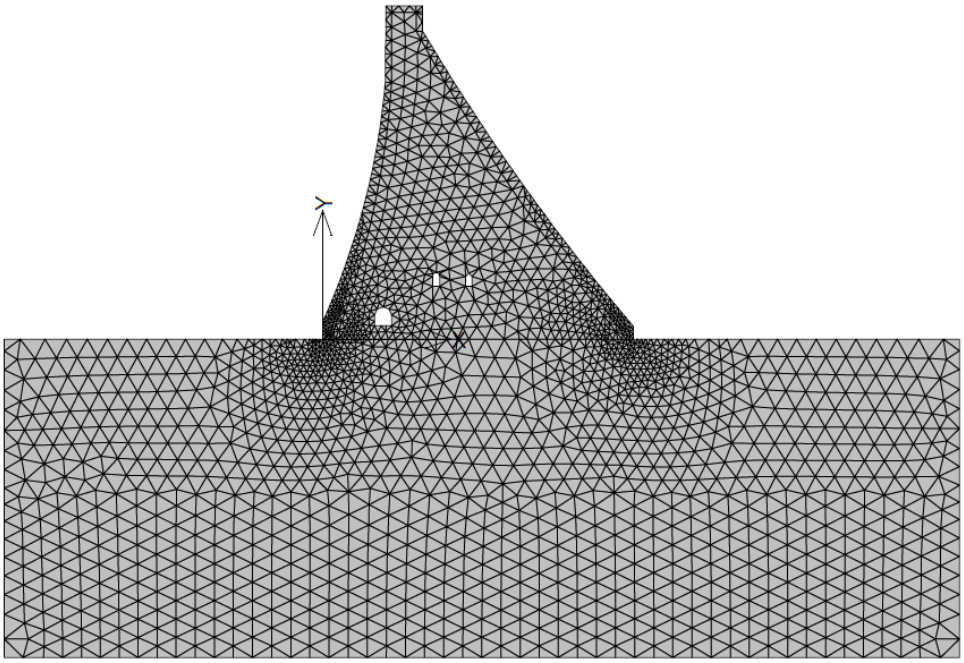

Figure 4.2 - Mesh used on the model

4.3 MATERIAL PROPRIETIES

This section presents the nonlinear characteristics of masonry and rock as well as the way in which they were implanted in ATENA 2D. For this model, the deformations of the materials are defined as “Plane Strain idealization” in order to preserve a deformation according to the xy plane.

4.3.1 Modelling of masonry

In the case of masonry, there are two typical analysis approaches: macro-modeling and micro-modeling. A macro-modeling is selected in this case. This choice is explained by the fact that masonry has orthotropic material properties due to the presence of mortar joints which act as planes of weakness. The use of hollow masonry units and the partial injection of voids increase the degree of complexity of the material characteristics. With macro-modelling, the model is considered as a homogeneous body using global masonry properties. As each part of the model represents the homogenized properties of the masonry, each element must include at least a part of the masonry units and the mortar. Moreover, a coarser mesh (fewer elements) is necessary, which reduces the computation time.

The section of the dam is modeled as a macro-element with the properties of the material "3D Nonlinear Cementitious2". This plastic and fracture material model combines constitutive models for tensile (failure) and compressive (plastic) behavior described in detail by Cervenka and Jendele (2010). An incremental formulation is used instead of a total formulation for the fracturing part of the model, which makes it possible to use this material for the creep calculation as in the case of the present study.

The young's modulus E derived from the recommendations of the Italian code. For the rest, tests were carried out on the dam in 2000-2015 and their results are referenced in the technical report. They identify some linear proprieties such as the density ρ and the Poisson’s ratio ν and all required non-linear properties such as compressive strength f_c, tensile strength $f_t$and tensile fracture energy G_f.

	Young's modulus; E[mpa]	Poisson' ratio; ν	Tensile strength; f_t[mpa]	Compressive strength; f_c[mpa]	Tensile fracture energy; G_f[MN/m]	Density; ρ[MN/m3]
Rubble	1500	0,26	1,6	25,33[1]	5,00E-05	2,30E-02
Ashlar	2850	0,26	1,6	25,33	5,00E-05	2,60E-02

(1) Cubic compressive strength f_{cu}= 29,8 MPa

Table 4.1 - Properties of masonry units

Crack spacing; S_{max}[m]	Tension stiffening; c_{ts}[m]	Plastic strain at strength; $f_c\ \varepsilon_{cp}$[-]	Critical compressive displacement; w_d[m]	Crack shear stiffness factor; S_F[-]	aggregate size; [m]
5,00E-3	0,4	-5,00E-03	-5,00E-03	20	2,00E-02

Table 4.2 - Additional properties of masonry units

4.3.2 Rock mass and joint modelling

The rock mass is represented as a monolithic structure without any discontinuity and modeled as a plastic body following the Drucker-Prager law with the properties of the material "3D Drucker-Prager Plasticity". In the case of the rock mass, the values of the linear properties such as the density ρ, the Young's modulus E and the Poisson's ratio ν are taken from the technical report carried out on the rock mass of the Janov, all based on laboratory results from core samples take between years 2000 and 2015.E is also supported by pressiometric in-situ tests. For this material, other properties must be entered such as the Drucker-Prager criterion and the Drucker-Prager parameter derived from the following relations:

$$\alpha_{DP} = \frac{2\sin\Phi}{\sqrt{3}\,(3+\sin\Phi)} \quad ; \quad \mathrm{K} = \frac{6\cos\Phi}{\sqrt{3}\,(3+\sin\Phi)} \qquad equation\ 10$$

With Φ= value of the angle of internal friction given in the technical report.

Young's modulus; E[MPa]	Poisson' ratio; ν	Density; ρ[MN/m3]	Tensile strength; f_t[MPa]	Compressive strength; f_c[MPa]	Drucker-Prager criterion; α_{DP}[-]	Drucker-Prager parameter; K [MPa]	Critical compressive displacement; w_d[m]
1000	0,25	2,60E-02	2	20 [1]	0,2[2]	7,30E-01[2]	-5,00E-03

(1) Cubic compressive strength f_{cu}= 29,8 MPa

(2) Angle of internal friction Φ= 40°

Table 4.3 - Rock properties

The joint represents the connection between the dam and foundation. ATENA 2D offers 3 types of connections: no connection, a rigid connection and a Mohr-Coulomb connection represented by the "2D interface material". It is this last type of connection that is selected. The table 4.5 gives the components of the interface material, which describes the physical properties of the contact between the macro-elements.

The properties of the interface material between the dam and its foundation are derived from the previously cited technical report as well as from the literature “Static and Coupled Hydro-mechanical Analyzes of Concrete Gravity Dam resting on Jointed Rock Foundation” (Rampal, A ., Halder, P., Manna, B. et al, 2020).

Normal stiffness; K_{nn}[GPa/m]	Normal stiffness; K_{nn} [MN/m3]	Shear stiffness; K_{tt}[GPa/m]	Shear stiffness; K_{tt}[NM/m3]	Tensile strength; f_t[MPa]	Friction coefficient; μ[-]	Joint cohesion; c[MPa]
2	2000	0,2	200	0,2	0,84	0,1

Table 4.4 - Properties of the interface material between the dam and its foundation

4.3.3 Model limit conditions

In order to reproduce the in-situ conditions, the physical representation of the boundary conditions is considered as follows: the sides of the foundation block have been restrained to the boundary conditions of the roller, which means locked in the x direction and free in the y direction. The base of the foundation block was completely blocked by constraining the vertical and horizontal directions.

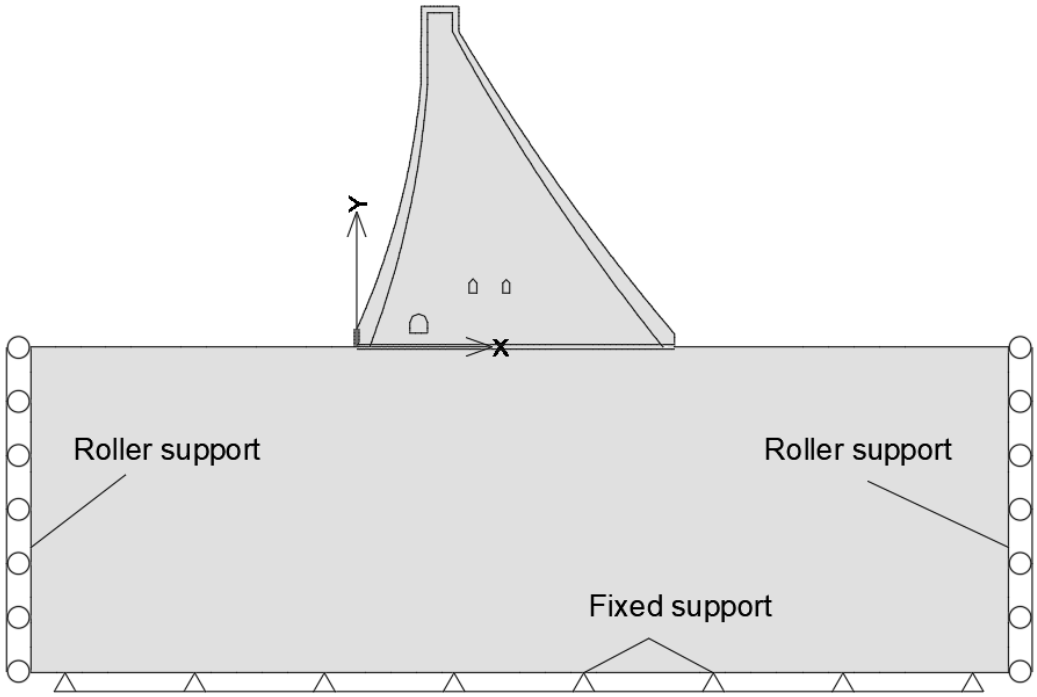

Figure 4.3 - Boundary conditions in stress analyses, illustrated with arrows

4.4 STATIC LOADS

Static loads (gravity load, earth pressure, water pressure, sediment pressure and uplift pressure) were applied in a single step.

Two permanent loads are to be considered, the gravity load of the dam body and the rock mass on which it rests, as well as the earth pressure applied to it. The gravity load values applied to the body of the dam can be found in table 4.2 and that of the rock comes from the technical report.

$$\gamma_{rm} = 2{,}30E-2\ MN/m^3 \quad ; \quad \gamma_{ash} = 2{,}60E-2\ MN/m^3 \quad ; \quad \gamma_{rock} = 2{,}60E-2\ MN/m^3$$

The formulation of the earth pressure as well as the loads applied to the dam change because they are no longer expressed as equivalent forces but as distributed. Earth pressure is defined locally on the downstream surface line. It takes the form of a quadrilateral distributed loading whose boundary values are given by the following relation:

$$F_{TH}(h_t) = \Upsilon_T\, h_t\, K_0 = \Upsilon_t\, h_t\, \frac{\nu}{1-\nu} = [0\,;0{,}16]\ MN/m^2 \qquad pour\ \ h_t = [0\,;8{,}91]\ m \quad equation\ 11$$

In the case of variable loadings, reservoir water is taken into consideration which induces water pressure, sediment pressure, and uplift pressure along the dam-foundation interface. The push of the water is expressed with a single formulation, its distribution is local along the surface of the dam upstream. The water level was defined from the base of the dam to its 49,24 m of height, the boundary values of which are given by the following relationship:

$$E_{am}(h_{am}) = \rho_E\, g\, h_{am} = [0\,;0{,}49]\ MN/m^2 \qquad pour\ \ h_{am} = [0\,;49{,}24]\ m \qquad equation\ 12$$

The sediment thrust follows the same distribution as the water pressure but its level stops at the upstream land line and its formulation is expressed as follows:

$$F_{sed}(h_{sed}) = \Upsilon_{sed}\, h_{sed} = [0\,;0{,}12]\ MN/m^2 \qquad pour\ \ h_{sed} = [0\,;11{,}4]\ m \qquad equation\ 13$$

As presented in part 3.2 (Action and Solicitation) this present study takes into account the effect of the grout curtain and the drains; therefore, the distribution along the dam-foundation interface follows the non-linear model of the German standard (DIN 19700):

$$S_{am}(b_x) = H_F\, \rho_E\, g = [0{,}49\,;0{,}49]\ \ MN/m^2 \qquad pour\ \ b_x = [0\,;8{,}4]\ m \qquad equation\ 14$$

$$S_{am}(8{,}4) = 0{,}60\ H_F\, \rho_E\, g = 0{,}29\ \ MN/m^2 \qquad and\ \ S_{am}(50{,}98) = 0{,}00\ \ M\,N/m^2 \qquad equation\ 15$$

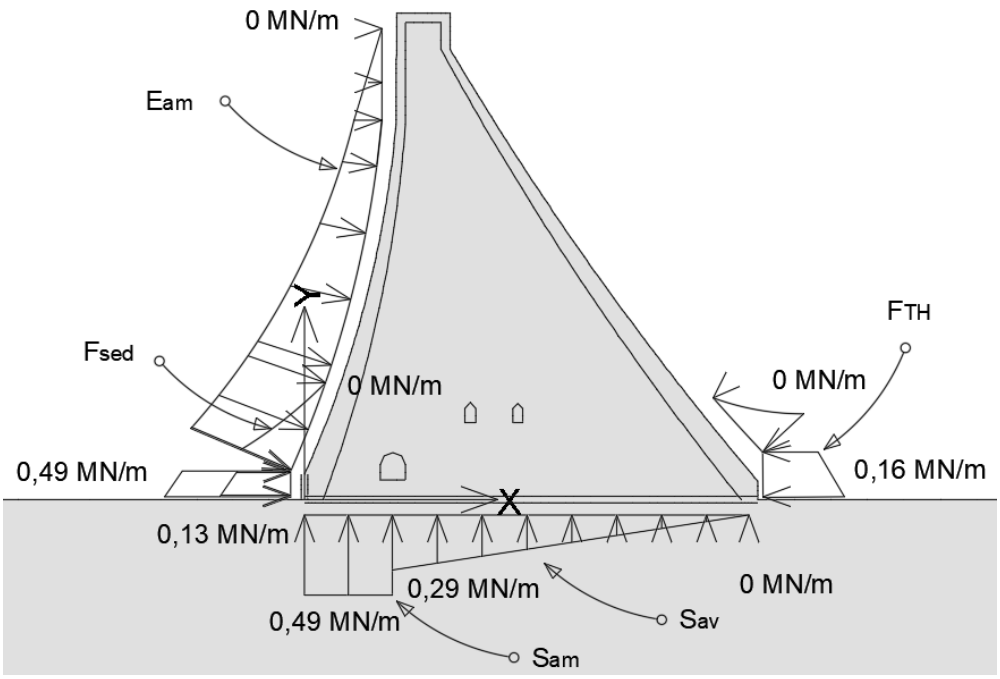

Figure 4.4 - Distribution of forces and actions applied to the model

4.5 THERMIC LOAD

Figure 4.5 shows the temperature distribution in the dam and rock base in winter and summer. The entire model was subjected to an initial temperature of 3,00°C, which corresponds to the unconstrained temperature. Temperatures were applied to the faces of the geometry using temperature fields. The table 4.6 presents the thermal expansion coefficient values introduced for each material of the model. The surfaces exposed to the air received the air temperature which varies between 0,00 and 20,00° depending on the season studied and the bottom was subjected to a constant temperature of 3,00°C.

material	Coefficient of thermal expansion; α [1/K]
Masonry	7,00E-6
Rock	4,00E-6

Table 4.5 - material data for the calculation of the temperature flow

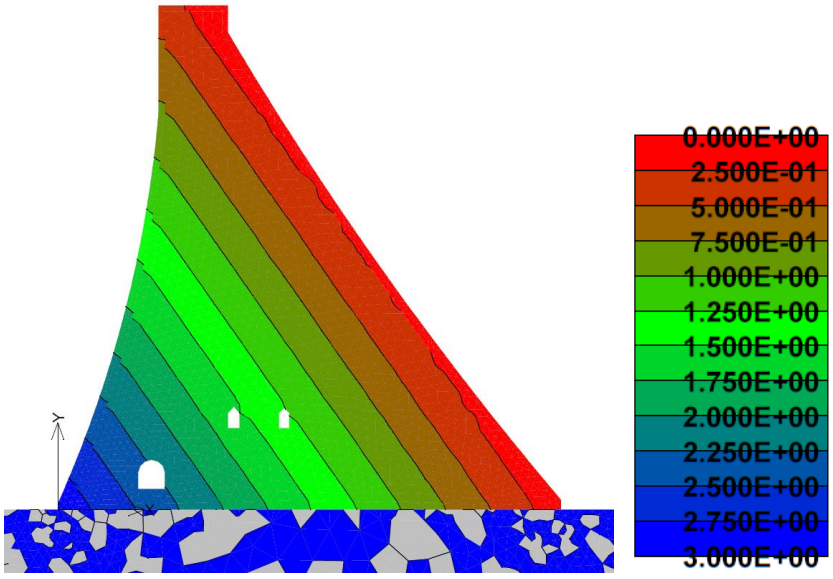

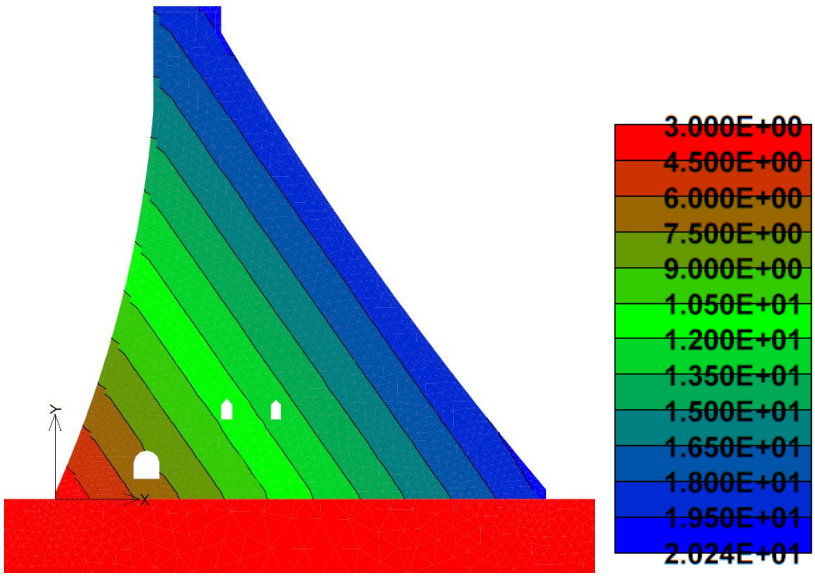

Figure 4.5 - Temperature distribution (in °C) inside the dam: (a) in winter; (b) in summer.

5 MODEL EVALUATION

This section aims to evaluate the dam-foundation system in the case of the static loading presented in part 4.4 as well as of the thermal loading presented part 4.5.

The results studied are the generation of stresses and the displacement along the vertical plane of the dam-foundation system. For comparison, an elastic model was also carried out in order to assess the validity of the results of the nonlinear model. The dam-foundation interface is defined as "rigid" and the tables 5.1 and 5.2 present the properties of this model.

	Young's modulus; E[MPa]	Poisson's ratio; ν	Density; ρ[NM/m3]
Rubble	1500	0,26	2,30E-02
Ashlar	2850	0,26	2,60E-02

Table 5.1 - Elastic properties of the masonry elements of the dam

Young's modulus; E[MPa]	Poisson' ratio; ν	Density; ρ[MN/m3]
1000	0,25	2,60E-02

Table 5.2 - Elastic properties of the rock

5.1 STRESSES ASSESSMENT

Figures 5.1 and 5.2 present the typical minimum (compression) and maximum (tensile) principal stress contours for the nonlinear and elastic models.

In the case of minimum principal stresses (compression):

Within the dam, large stress flows move from the upstream face to the downstream face in a fairly constant manner. These stresses are due primarily to the gravity load of the dam, which explains why the compression values are lowest at the level of the crown and gradually increase when approaching the base of the dam. These stresses are also due to hydrostatic loading, which causes an increase in stress along the upstream surface. Stress concentrations also appear around galleries.

At the base of the dam, a concentration of stresses forms at its downstream toe. This reaction is due to water pressure applied upstream and the uplift pressure causing the dam to tilt in the downstream direction. These phenomena are similar between the elastic model and the non-linear models but at different scales. The stress concentration at the downstream toe of the dam is higher for the elastic model by 53%. This difference is due to the integration of the interface in the non-linear model which allows the sliding of the dam on its base and decompressed the compression zone.

In the case of maximum principal stresses (tensile):

Within the dam, four major stress flows leave from the upstream face to converge at the level of the downstream toe of the dam. These stresses are also due to the water pressure which stretches the dam in the downstream direction. The triangular shape of the dam generates an increase in these tensile stresses towards the crown. Graphically, these phenomena are only perceptible in the case of the non-linear model but are considered similar on the elastic model.

At the base of the dam, the uplift pressure caused by the hydrostatic loading generates a maximum uplift effect at the level of the upstream toe and which decreases until it disappears at the level of the downstream toe of the dam. This effect is very marked on the elastic model with a high concentration of stress at the upstream toe with a difference of 800% with the non-linear model. This difference is due to the integration

of the interface in the non-linear model which allows the lifting of the dam and therefore the redistribution of this tensile stress along the foundation.

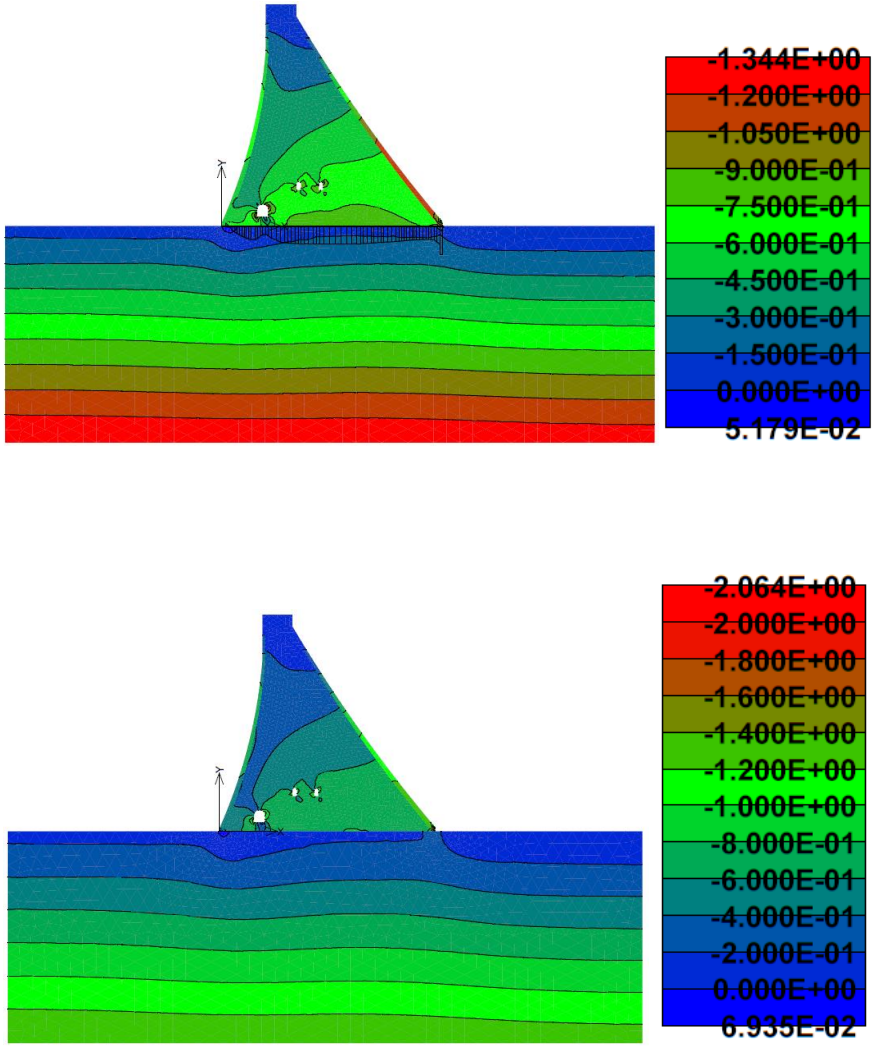

Figure 5.1 - Min principal stress contours for the dam-foundation system: (a) non-linear model; (b) elastic model

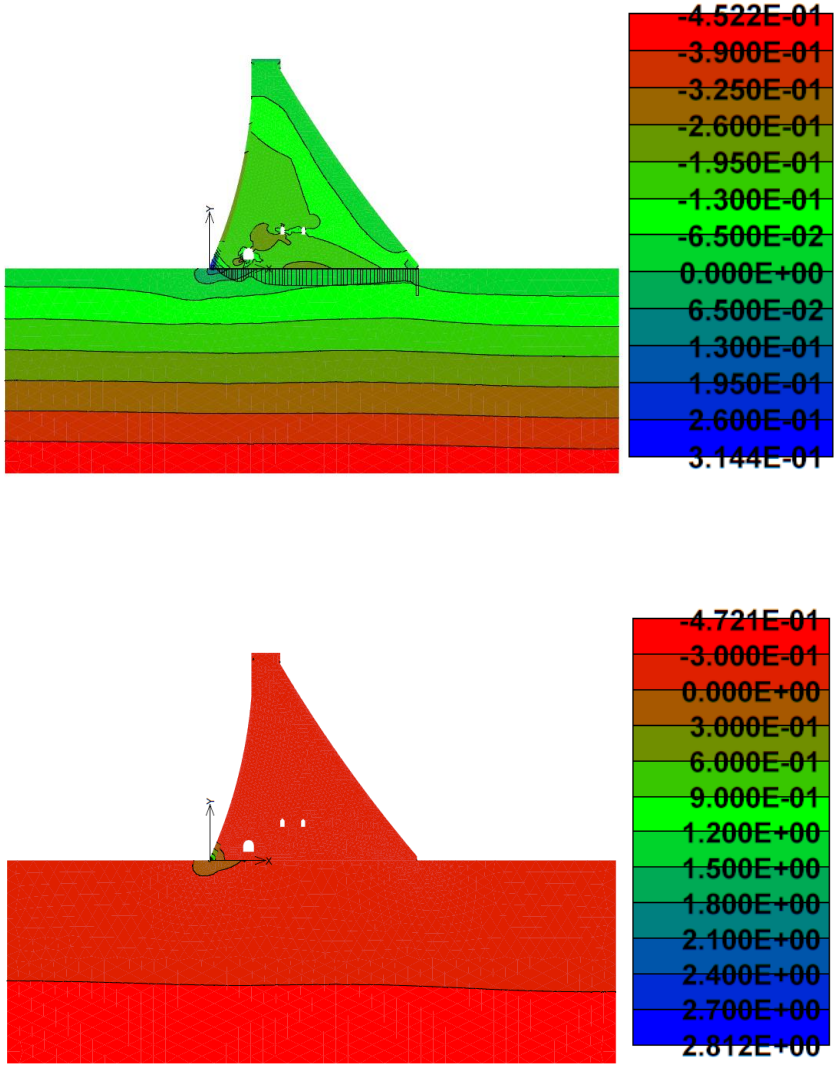

Figure 5.2 - Maximum principal stress contours for the dam-foundation system: (a) non-linear model; (b) elastic model.

Figure 5.3 compares the normal stresses σyy obtained analytically in part 3.2 (Actions and Solicitations) and those of the non-linear model along the interface of the dam:

Tensile stresses first appear at the upstream toe. The values between the two models are almost identical with a difference of 30%. The offset of the non-linear model corresponds to the uplift of the dam allowed by the interface. A first difference is marked between the models with the rapid increase in the compressive stresses of the non-linear model due to the effect of the grout curtain and the drains. A plateau is then observable in the case of the non-linear model up to the edge of the downstream toe of the dam. The normal stress of the non-linear model is 80% greater than the analytical response.

It can be concluded that the analytical method underestimates the magnitude of the stress compared to the non-linear model because it does not take into consideration geometric irregularities.

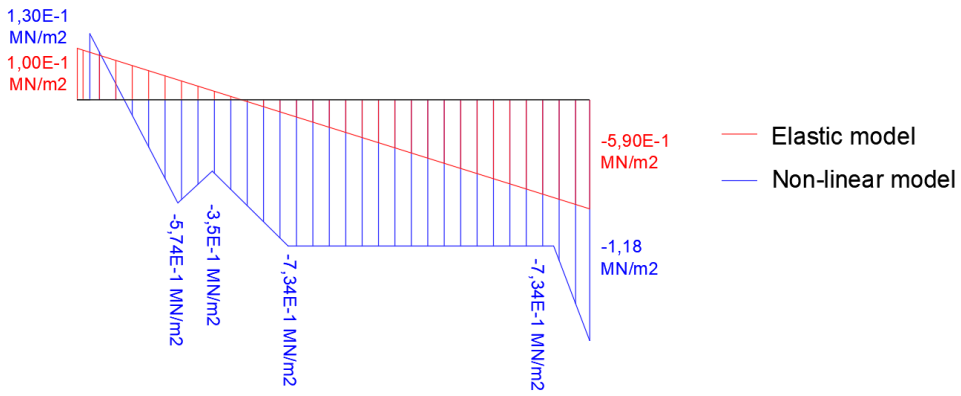

Figure 5.3 - Normal stresses σyy along the dam-foundation interface

5.2 DISPLACEMENT ASSESSMENT

Figure 5.4 presents the contours of the horizontal displacements due to hydrodynamic loading for the non-linear and elastic models.

The deformation of the dam includes the following three deformation components: (i) the deformation of the monolithic dam; (ii) deformation of the monolithic rock; (iii) the slip displacement along the rock joint in the case of the non-linear model.

The hydrostatic loading applied to the upstream surface causes the progressive displacement of the arcs of the dam downstream, accompanied by a tilting of the consoles downstream around the toe of the dam. The triangular shape of the dam causes a gradual increase in the horizontal displacement towards the crown. The displacement differences are almost negligible between the elastic and non-linear models with an increase of 14% for the latter at the level of the crown. This difference is due to the lifting of the dam which allows more movement downstream.

The deformation of the monolithic rock develops as an extension of the displacement of the dam while remaining concentrated under it. Contrary to the rock of the elastic model which moves under the whole of the interface, the rock of the non-linear model does not move at the points upstream and downstream under the thickness of ashlar. This difference is explained by the lifting of the dam upstream.

In the case of the dam sliding along the joint of the rock, a break in the displacement is observed at the level of the interface. The shear stiffness of the interface plays a decisive role on this horizontal displacement value between the dam and its foundation.

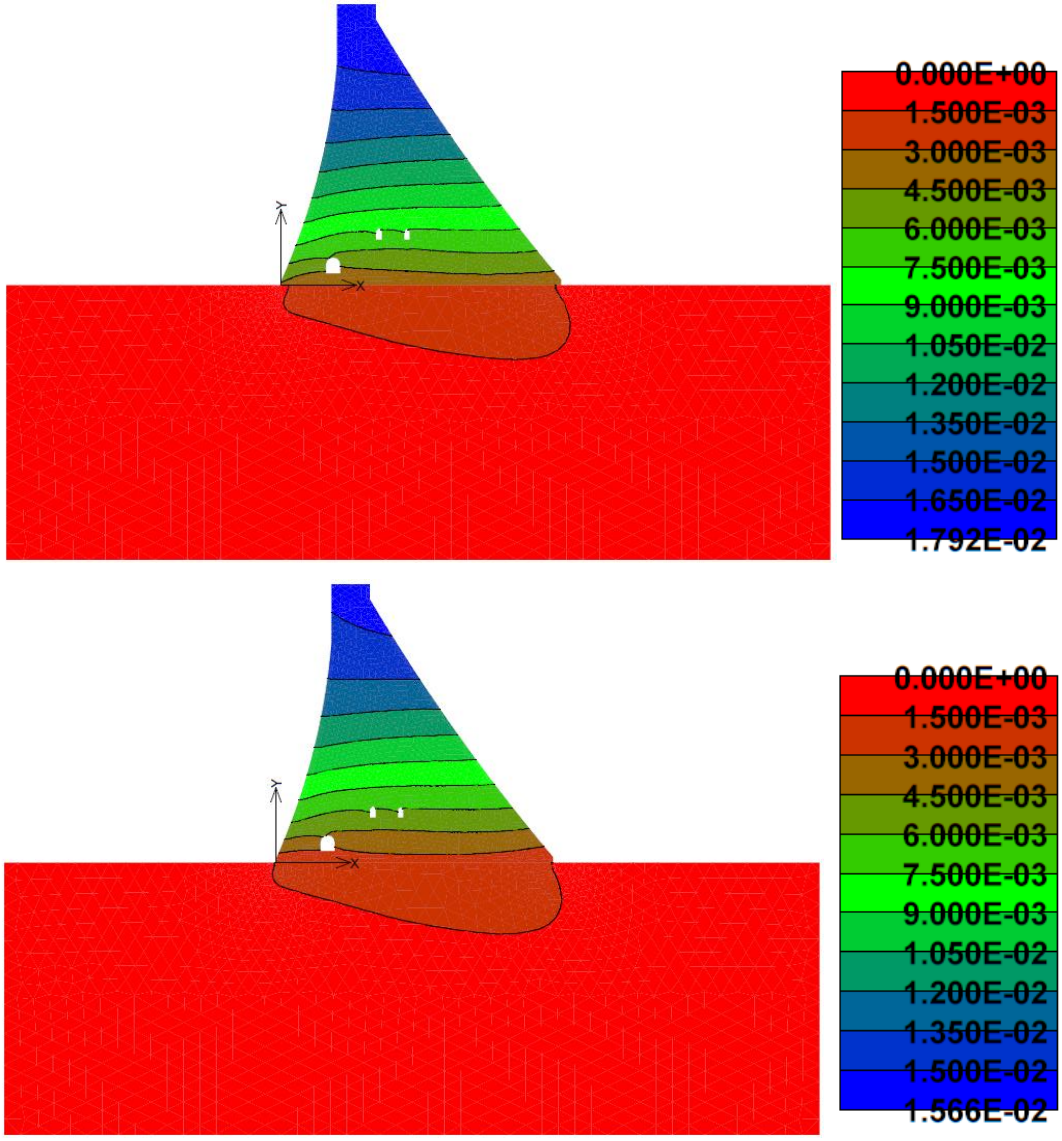

Figure 5.4 - Contour of horizontal displacements under static loading: (a) non-linear model; (b) elastic model.

Figure 5.5 presents the contours of the horizontal displacements due to the thermal loading on the non-linear model in winter (0°C) and in summer (20°C). The comparison of the values shows a general upstream displacement greater in summer of 55%. This tendency is due to the expansion of the dam body.

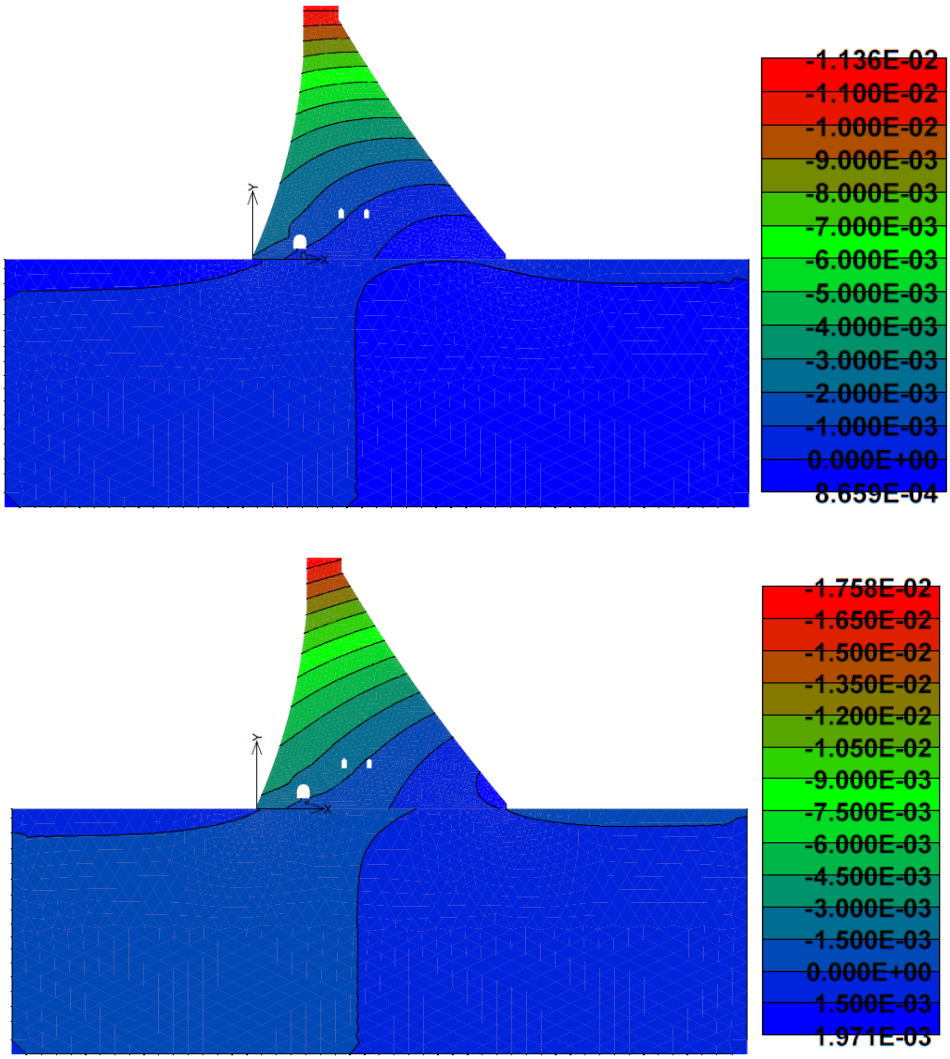

Figure 5.5 - Contour of horizontal displacements under thermal loading: (a) for 0°C; (b) for 0°C

6 MODEL CALIBRATION

In order to monitor the structural integrity of the Janov dam, a Huggenberg GL50–100 pendulum pendulum was installed in its central tower. In this section, INSITU results from the pendulum will be used to calibrate the masonry components of the dam.

Figure 6.1 shows the section of the dam where the Huggenberg GL50 – 100 pendulum was installed.

Along this pendulum are three monitored points (KK84(1), KK84(2) and KK84(3)) and the pendulum reference point (FP) whose coordinates are specified. These points give in real time the deformation of the dam along the horizontal plane. These displacements are relative and defined according to the pendulum reference point whose displacement is defined as zero.

Within the framework of this study, only displacements in the upstream and downstream directions are considered, the directions perpendicular to the watercourse are neglected.

The deformation of this pendulum depends mainly on the temperature, the load and the position of the water surface. This is why two independent studies are carried out, (i) the first is based on the analysis of the constraints (gravity load, earth pressure, water pressure, sediment pressure and uplift pressure); (ii) the second only takes thermal analysis into account; (iii) From these two calibrations, a unique model will be proposed.

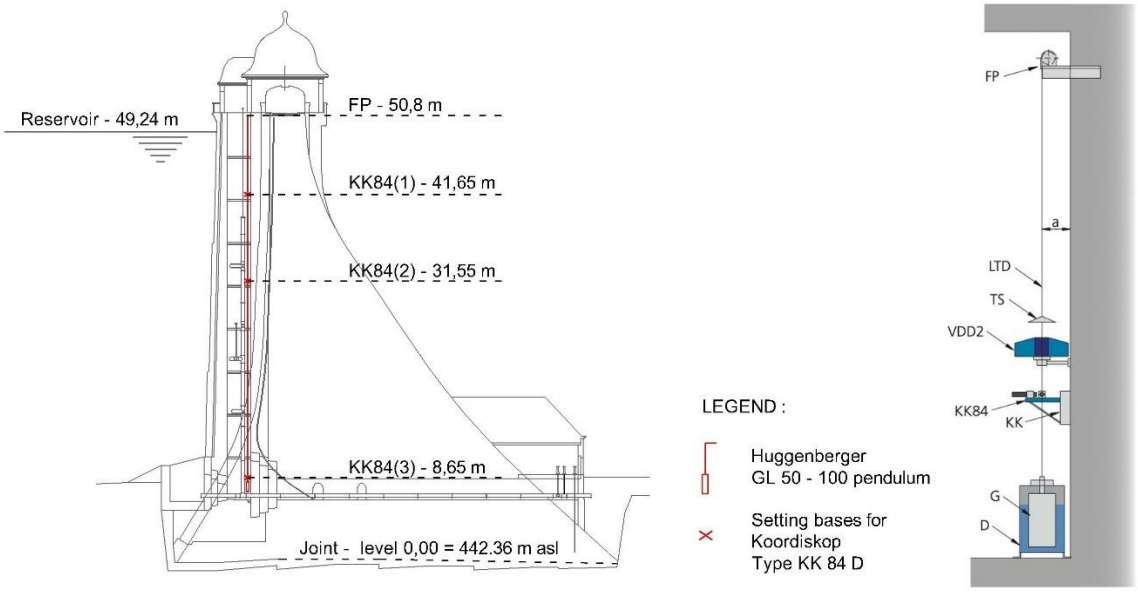

Figure 6.1 - pendulum: (a) monitoring points coordinate © Technical report; (b) model utilized. Legend: FP the pendulum reference point, LTD the pendulum wire, G the pendulum weight and D the damping vessel, VDD2 The contactless remote measuring instrument Telelot, KK84 Coordiscope For manual measuring.

6.1 CALIBRATION WITH STRESS ANALYSIS

For the stress analysis, only the static loads (gravity load, earth pressure, water pressure, sediment pressure and uplift pressure) are applied to the model.

The calibration will be carried out on the basis of IN-SITU data collected on the dam in 2010-2015 and transcribed in the technical report. Table 6.1 presents the results of the linear regression model carried out on the basis of these data. In the case of an increase in the water level of one meter, this model gives the displacement between the pendulum reference point (FP) and the monitoring points installed along the dam:

	PF	KK84(1)	KK84(2)	KK84(3)
Relative position [m]	0,00	1,47E-5	3,77E-5	1,26E-4

Table 6.1 - Prediction of relative positions of monitoring points.

This model informs us of the IN-SITU reaction of the deflection line of the dam during the modification of the hydrostatic loading and the uplift pressure which are intrinsically linked as presented in part 3.2 (Actions and Solicitations).

6.1.1 Loadings steps

The linear regression model carried out on the basis of IN-SITU data is defined in the case of an active loading on the dam. The deformation of the dam must therefore be studied between two loading states.

To do this, the calibration of the model will be between its minimum water level of 460 asl (17,6 m) and a maximum height of 49,24 m as shown in the figure 6.2:

For the first water level, self-weight, earth and sediment pressures are taken into account as defined in part 4.4 (Static loads) The water pressure and the uplift pressure are redefined as follows:

The formulation of the water pressure is the same as in part 4.4:

$$E_{am}(h_{am}) = \rho_E \, g \, h_{am} = [0\,;0{,}17]\ MN/m^2 \quad pour\ \ h_{am} = [0\,;17{,}6]\,m \qquad equation\ 16$$

In the case of uplift pressure, it was previously assumed that the magnitude of the data was based on the German standard model (DIN 19700) which puts us in the worst-case scenario. During work on the dam in 2010-2015, water pressure values were collected at the joint, upstream and downstream and at a given water height. These data made it possible to obtain two linear regression models:

$$UP_{am} = 0{,}942598\ W_S + 16{,}94 = 81\ WC$$
$$UP_{am} = 0{,}081\ MN/\,m^2 \qquad (uplift\ pressure\ upstream)\ equation\ 17$$

$$UP_{av} = 0{,}589803\ W_s + 174{,}05 = \ 30\ WC$$
$$UP_{av} = 0{,}03\ MN\ /\ m^2 \qquad (uplift\ pressure\ downstream)\ \ equation\ 18$$

With WC= 1 m of water column; W_s= height of water above sea level.

The definition of the upstream and downstream uplift pressure values changes compared to the German standard (DIN 19700) but the form is kept for the sake of simplification.

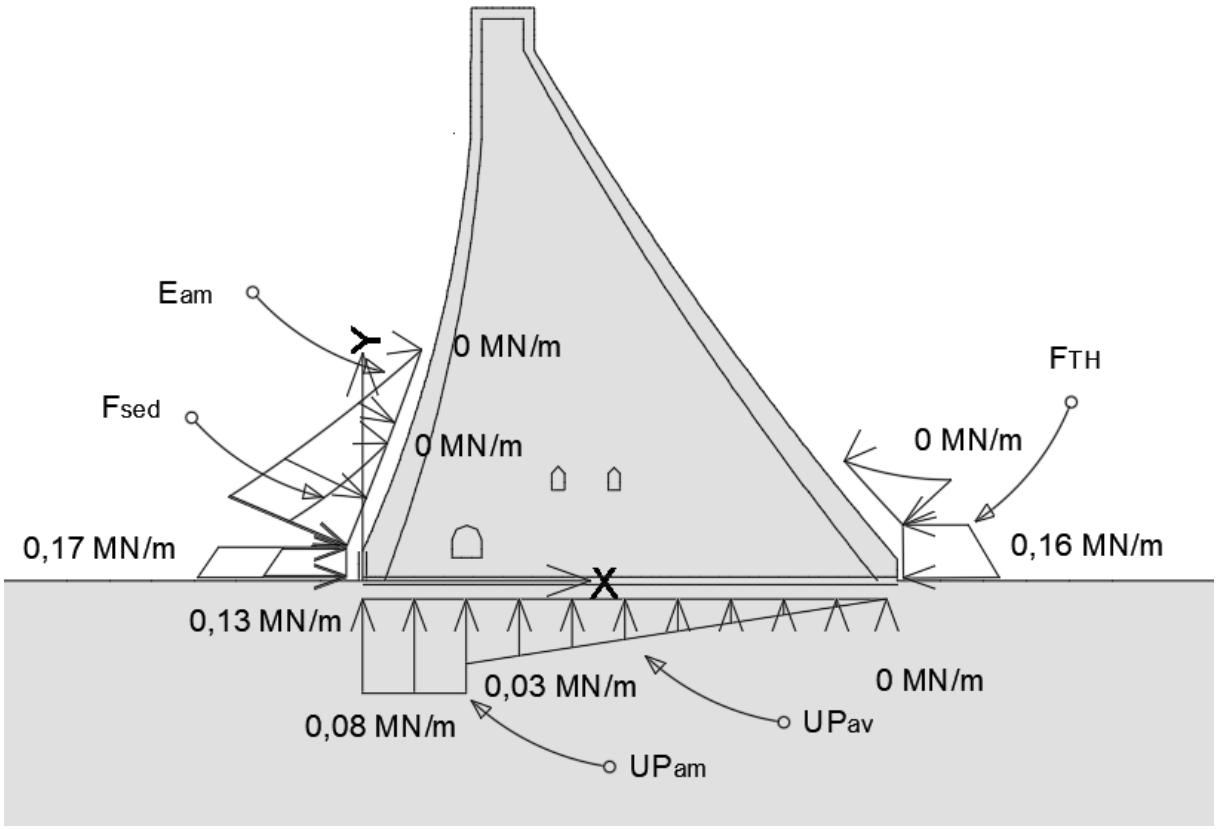

Figure 6.2 - Distribution of forces and actions applied to the model - step 1

For the second water level, gravity load, earth pressure and sediment pressure are neglected so that ATENA does not count them twice. In the same way, the previously calculated water pressure and uplift pressure have been removed from this new load.

$$E_{am}(h_{am}) = [\,0; 0{,}315; 0{,}315]\ MN/m^2 \quad pour\ \ h_{am} = [0\,;\,17{,}6\,;\,49{,}24]\ m \qquad equation\ 16$$

$$UP_{am} = 0{,}298\ MN/m^2 \qquad equation\ 17$$

$$UP_{av} = 0{,}186\ MN/m^2 \qquad equation\ 18$$

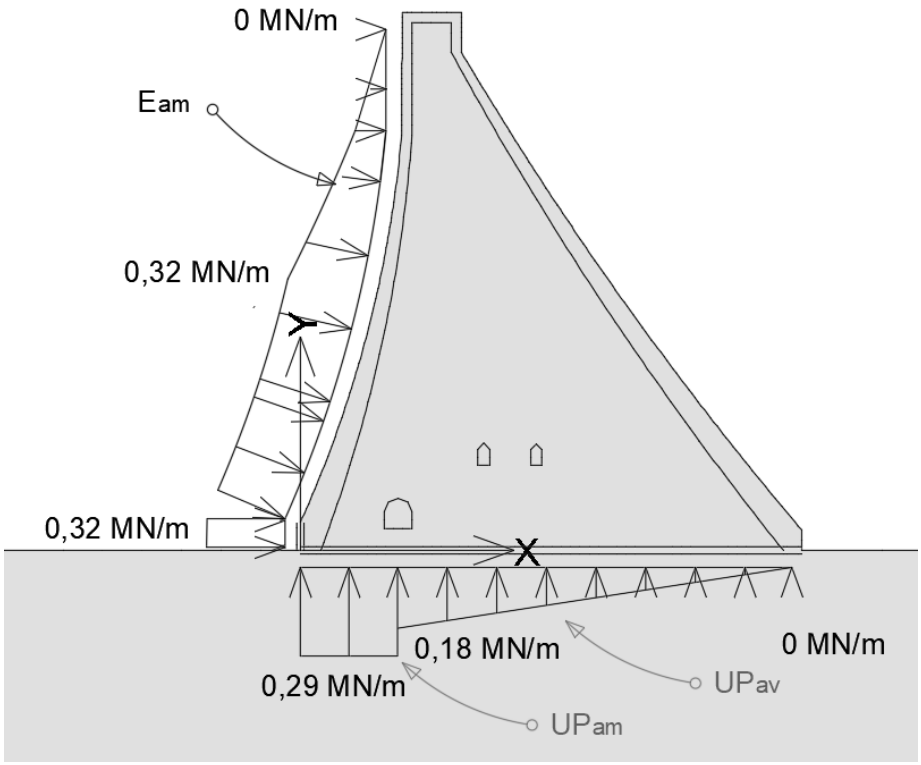

Figure 6.3 - Distribution of forces and actions applied to the model - step 2

The deflection line of the dam is then studied between these two loading stages and compared to the IN-SITU data taken from the pendulum. The table 6.2 provides us with the relative vertical displacement of each monitoring point targeted for the calibration of the model. These data are obtained thanks to the following relationship:

$$M1 = (FP - KK84(1)) * H_{diff} = 4{,}60E - 4\ m \qquad equation\ 19$$

$$M2 = (FP - KK84(2)) * H_{diff} = 1{,}10E - 3\ m \qquad equation\ 19$$

$$M3 = (FP - KK84(3)) * H_{diff} = 4{,}00E - 3\ m \qquad equation\ 19$$

With H_{diff}= Differential height between the two water heights studied

	PF	M1	M2	M3
Relative displacements [m]	0,00	4,60E-4	1,10E-3	4,00E-3

Table 6.2 - Relative vertical IN-SITU displacements between the monitoring points.

6.1.2 Results and calibration

In the initial state, the components materials of the model are based on the results of the tables 4.2 , 4.3 , 4.4 , 4.6 of the part material properties 4.3. Monitoring points are positioned along the model, at the same heights as the IN-SITU sensors of the pendulum presented in figure 6.1.

The goal is to make the deformation of the model converge as much as possible towards the relative displacement M3, between the points FP and KK84(3), of the table 6.2. For this, the choice was made to play only on the modulus of elasticity of the masonry rubble. And then find another parameter on which to play to make the model converge towards the other relative displacements (M1 and M2).

Figure 6.4 shows the convergence of the relative displacements M1, M2, M3 according to the Young's modulus of the masonry. It can be seen that a 1233% increase in the Young's modulus of the masonry, compared to the initial state, causes M3 to converge towards a value of 1,14E-2 m, i.e. a reduction of 28% and a difference of 65% with the target value (4,00E-3 m).

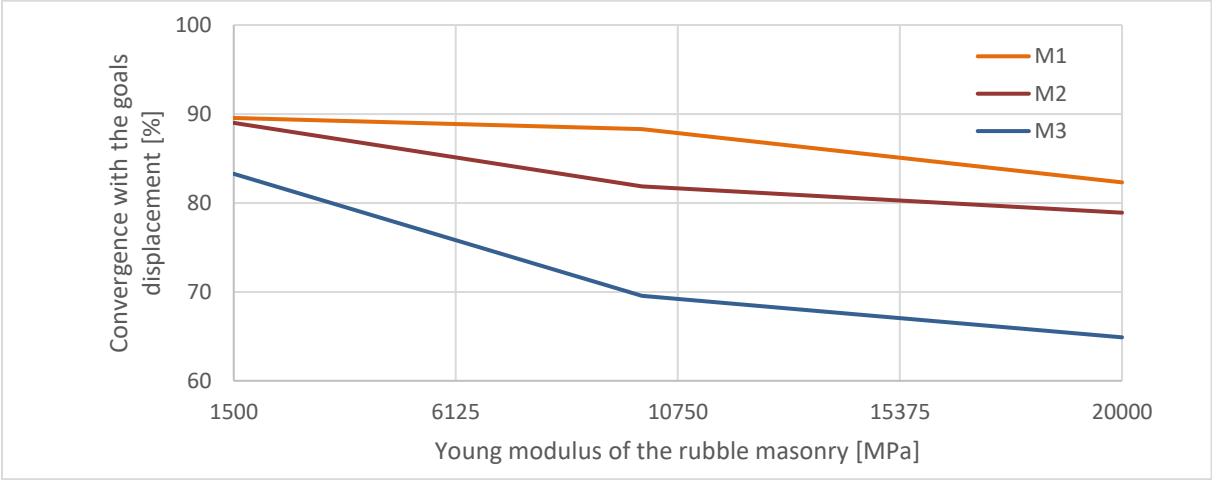

Figure 6.4 - Relative displacements between monitoring points of the model.

The reduced impact of the Young's modulus of the masonry on the deformation is due to the subsidence of the rock under its gravity load and that of the dam. This impact is very largely overestimated by the model which does not take into account the contribution of the 3D effect. To counteract this subsidence effect, the thickness of the section of the rock mass is defined equal to 100 m. This new geometry makes it possible to better approximate the behavior of the semi-infinite medium that constitutes the foundation.

Figure 6.5 shows the convergence of the relative displacements M1, M2, M3 according to the Young's modulus of the masonry for this new model. It can be seen that a 400% increase in the Young's modulus of the masonry, compared to the initial state, causes M3 to converge towards the target value (4,00E-3 m).

Displacements M1 and M2 converge by significant differences of 55% and 45% with the target values (4,60E-4 m and 1,1E-3 m). This difference is due to the geometry of the dam, finer at the level of the crown. The hydrostatic loading has a strong impact on the deformation of this part. The crown stiffening experiment by increasing the Young's modulus of Ashlar did not show satisfactory results.

The deduction is made that, as for the rock base, the contribution of the 3D effect, not taken into account in this model, would have the effect of reinforcing the upper part of the dam and therefore of better approximating the IN-SITU deformations.

The final calibration of the mechanical part gives a Young's modulus of the masonry equal to 7500 MPa.

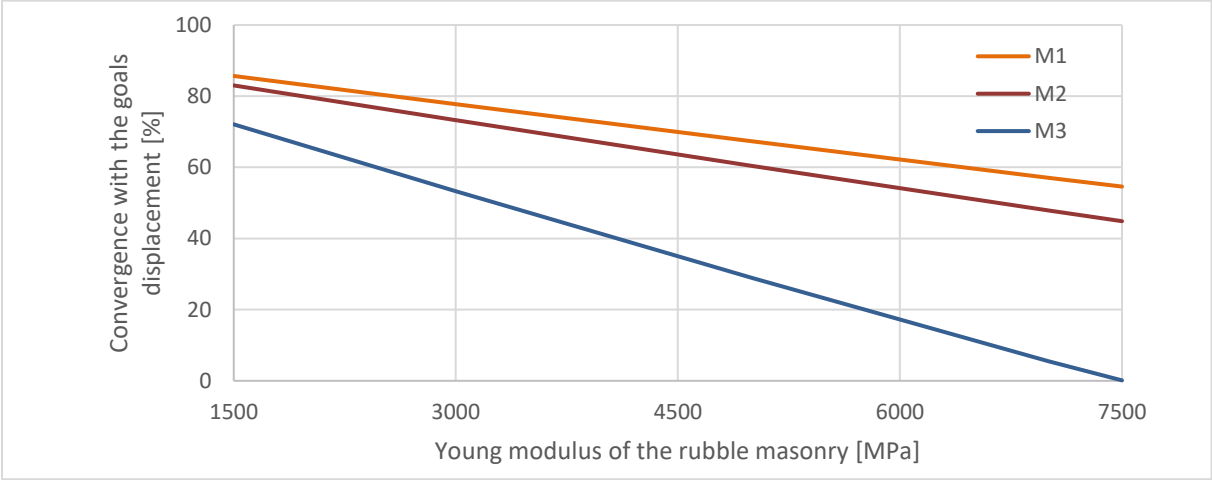

Figure 6.5 - Relative displacements between monitoring points of the model

6.2 CALIBRATION WITH THERMAL ANALYSIS

For the thermal part, only the gravity load and the thermal loading are applied to the model. The calibration will be carried out on the basis of IN-SITU data collected on the dam in 2010-2015 and transcribed in the technical report.

Figure 6.6 shows the location of the monitoring point (T6) placed on the model; these coordinates correspond to those of the sensor placed IN-SITU in 2010-2015. This sensor was placed 1 meter from the downstream surface in the masonry in order to avoid capturing too fast temperature fluxes along the surface of the dam.

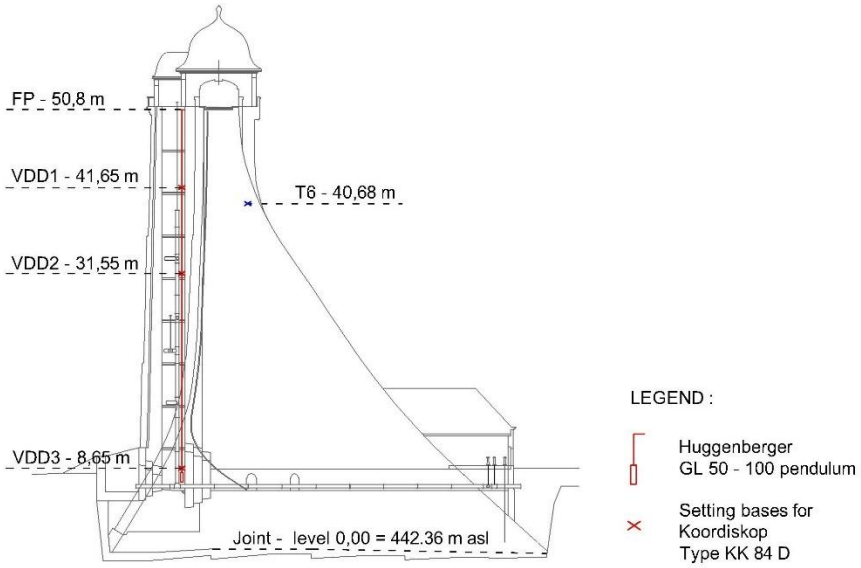

Figure 6.6 - monitoring temperature sensor coordinate, © Technical report.

Table 6.3 presents the results of the linear regression model carried out on the basis of IN-SITU data. In the case of a temperature increase of one degree at the level of the sensor, this model gives the difference in displacement between the pendulum reference point (FP) and the monitoring points installed along the dam:

	PF	KK84(1)	KK84(2)	KK84(3)
Relative position [m]	0,00	1,06E-4	2,44E-4	3,98E-4

Table 6.3 - Prediction of the relative positions of the monitoring points.

As for the stress analysis part, this model informs us of the reaction IN-SITU of the line of deflection of the dam during the modification of the thermal loading whose distribution is presented part 4.5 (Thermic load). The comparison with the deformations due to the hydrostatic loadings shows that the bending of the dam caused by the variations of temperature is greater by one order of magnitude.

6.2.1 Loading steps

The linear regression model performed on the basis of IN-SITU data is defined in the case of a temperature change of one degree at sensor T6. The deformation of the dam must therefore be studied between two temperature values.

To do this, the calibration of the model will be done between a first thermal loading of 15°C and a second of 16°C. The thermal loading is adapted so that these data are taken by the monitoring point T6.

For the first thermal loading, the own weight is taken into account. Figure 6.7.a shows the temperature distribution in the dam and the rock base in the case where T6 detects a temperature of 15°C.

For the second thermal loading, the own weight is neglected so that ATENA does not count it twice. Figure 6.7.b shows the temperature distribution in the dam and the rock base in the case where T6 detects a temperature of 16°C.

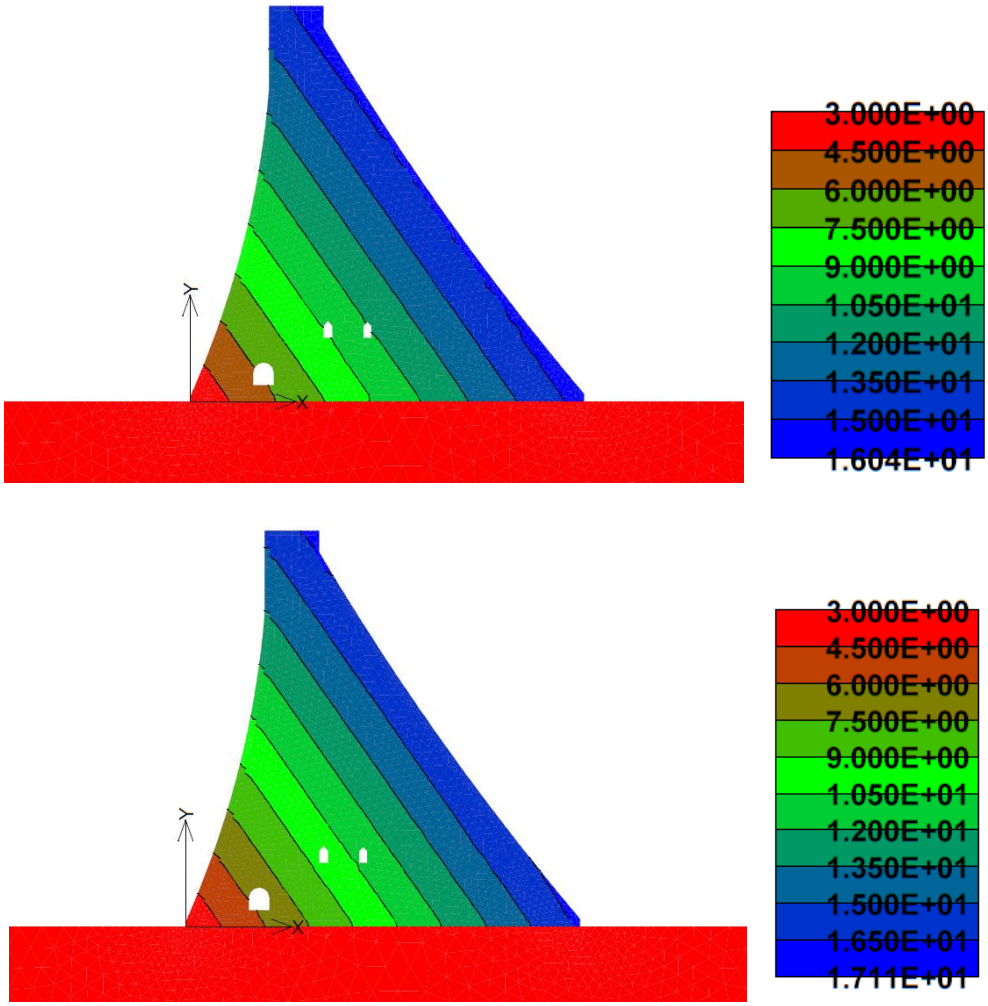

Figure 6.7 - Temperature distribution (in °C) inside the dam: (a) for T6 = 15°C; (b) for T6 = 16°C.

The deflection line of the dam is then studied between these two loading stages and compared to the IN-SITU data taken from the pendulum. The table 6.4 provides us with the relative horizontal displacement values of each monitoring point targeted for the calibration of the model. These data are obtained thanks to the following relationship:

$$M1 = VDD1\ T6_{diff} = 1{,}06E-4\ m \qquad equation\ 20$$

$$M2 = VDD2\ T6_{diff} = 2{,}44E-4\ m \qquad equation\ 20$$

$$M3 = VDD3\ T6_{diff} = 3{,}98E-4\ m \qquad equation\ 20$$

With $T6_{diff}$= Differential temperature between the two temperatures taken at point T6.

	PF	M1	M2	M3
Relative position [m]	0,00	1,06E-4	2,44E-4	3,98E-4

Table 6.4 - IN-SITU relative horizontal displacements of monitoring points for calibration.

6.2.2 Results and calibration

In the initial state, the components materials of the model are based on the results of the tables 4.2, 4.3 and 4.4 of the part 4.3 (Material properties) and the table 4.6 of the part 4.5 (thermic load). Monitoring points for the calibration of the part 6.2 (Stress analysis) are kept. An additional point is added to the coordinates of the sensor T6 shown in figure 6.6.

The goal is to make the deformation of the model converge as much as possible towards the relative displacements M1, M2 and M3, of the table 6.4. For this, the choice was made to play only on the modulus of elasticity of the masonry rubble to start and study the reaction of the model.

Figure 6.8 shows the displacement convergence of the values M1, M2, M3 as a function of the Young's modulus of the masonry. It can be seen that the modification of the Young's modulus has very little impact on the relative displacements of the monitoring points. By only varying this parameter, the vertical displacements M1, M2 and M3 do not converge and tend to oscillate respectively between [18; 52] %, [66; 75] % and [58; 63] % differences with their target values (1,06E-4 m, 2,44E-4 m and 3,98E-4 m).

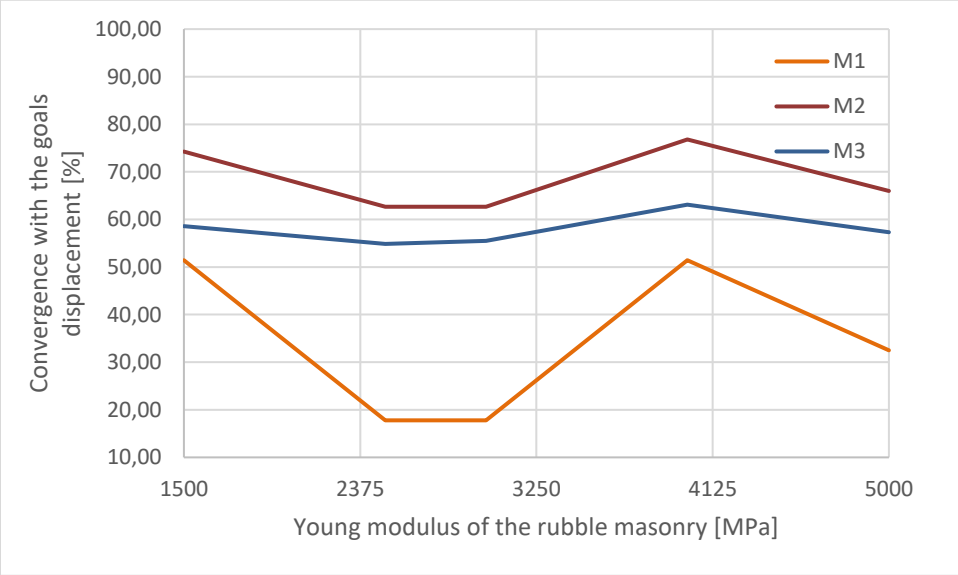

Figure 6.8 - Relative displacements between monitoring points of the model.

In addition to the Young's modulus of the masonry, the choice of a new calibration parameter focused on the thermal coefficient of expansion. This setting impacts how an object's size varies with temperature.

Figure 6.9 shows the displacement convergence of the values M1, M2, M3 as a function of the Young's modulus of the masonry and the thermal coefficient of expansion. It can be seen that a 170% increase in the Young's modulus of the masonry and a 70% increase in the thermal coefficient of expansion, compared to the initial state, causes M3 to converge towards the target value (3,98E-4 m). The values of M1 and M2 converge in the best case, respectively, towards differences of 11,5% and 6% with the target values (1,06E-4 m and 2,44E-4 m).

The final calibration of the thermal part gives a Young's modulus of the masonry equal to 4000 MPa and a thermal coefficient of expansion equal to 1,2E-5 1/K.

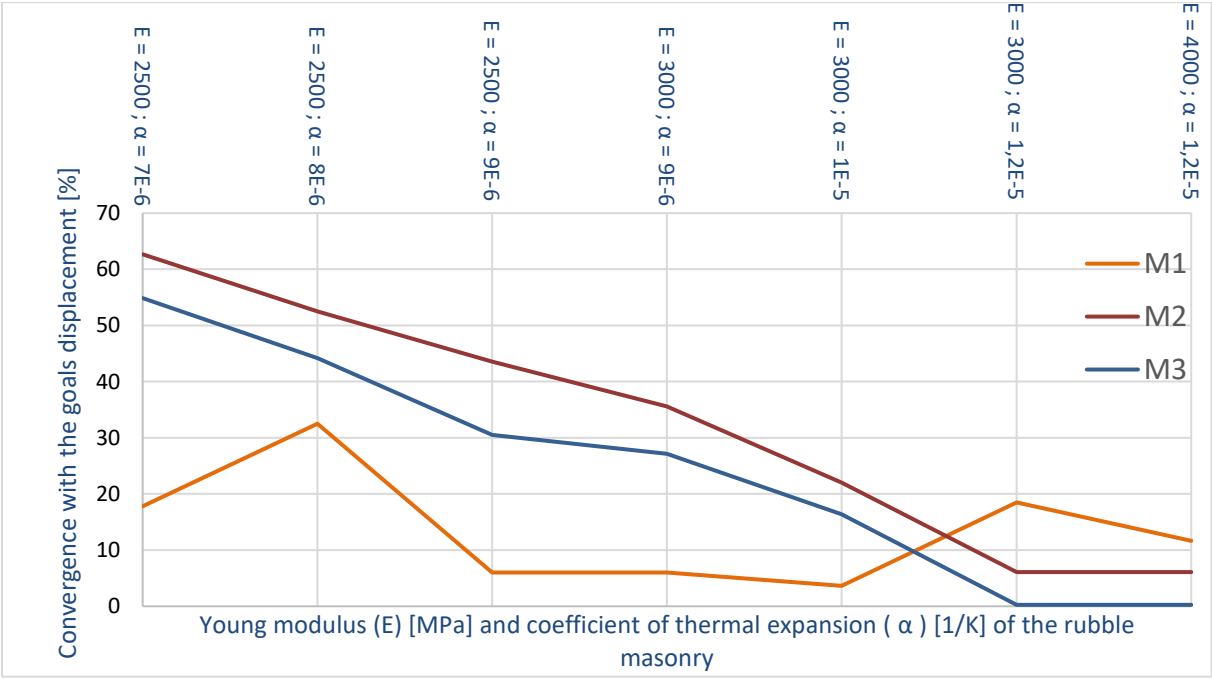

Figure 6.9 - Relative displacements between monitoring points

As mentioned in the "calibration with static stress" section, the contribution of the 3D effect (not taken into account in this model) would have the effect of reinforcing the upper part of the dam and therefore of better approximating the IN-SITU deformations. So, the calibration of the 2D model can't be based on the static load. Thermal calibration is much more promising, with better convergence of relative displacements and more realistic material properties. These results are therefore retained for the 2D model.

7 SUMMARY AND CONCLUSIONS

This thesis studies the effect of hydrostatic and thermal loading on the evolution of static stresses and strains in the Janov gravity dam, using a finite element model (FEM).

the main objectives of this study are to describe the model development process, including the generation of the model geometry and materials. Static and thermal loading analyses are then used to study the magnitude and nature of stresses and displacements at critical points in the dam. Finally, a comparison with IN-SITU data recovered from the dam enables the model to be calibrated. The work presented in this document has led to the following conclusions:

- Comparison of normal stresses between analytical calculation and non-linear model:

Tensile stresses first appear at the upstream toe. The values between the two models are almost identical with a difference of 30%. The offset of the non-linear model corresponds to the uplift of the dam allowed by the interface. A first difference is marked between the models with the rapid increase in the compressive stresses of the non-linear model due to the effect of the grout curtain and the drains. A plateau is then observable in the case of the non-linear model up to the edge of the downstream toe of the dam. The vertical stress of the non-linear model is 80% greater than the analytical response.

It can be concluded that the analytical method underestimates the magnitude of the stress compared to the non-linear model because it does not take into consideration geometric irregularities.

- The joint's role on the principal stresses:

In terms de compression, The stress concentration at the downstream toe of the dam is higher for the elastic model by 53%. This difference is due to the integration of the interface in the non-linear model which allows the sliding of the dam on its base and decompressed the compression zone.

In terms of traction, The stress concentration at the upstream toe of the dam is very marked on the elastic model with 800% difference with the non-linear model. This difference is due to the integration of the interface in the non-linear model which allows the lifting of the dam and therefore the redistribution of this tensile stress along the foundation.

- The joint's role on the displacement:

The hydrostatic loading applied to the upstream surface causes the progressive displacement of the arcs of the dam downstream, accompanied by a tilting of the consoles downstream around the toe of the dam. The displacement differences are almost negligible between the elastic and non-linear models with an increase of 14% for the latter at the level of the crown. This difference is due to the lifting of the dam which allows more movement downstream.

- Calibration with stress analysis:

The final calibration of the dam gives a Young's modulus of the masonry equal to 7500 MPa.

Displacement M3 converge towards the target value (4,00E-3 m). Displacements M1 and M2 converge by significant differences of 55% and 45% with the target values (4,60E-4 m and 1,1E-3 m). This difference is due to the geometry of the dam, finer at the level of the crown. The hydrostatic loading has a strong impact on the deformation of this part. The crown stiffening experiment by increasing the Young's modulus of Ashlar did not show satisfactory results.

The deduction is made that, the contribution of the 3D effect (not taken into account in this model) would have the effect of reinforcing the upper part of the dam and therefore of better approximating the IN-SITU deformations.

- Calibration with thermic analysis

In addition to the Young's modulus of the masonry, the choice of a new calibration parameter focused on the thermal coefficient of expansion. This setting impacts how an object's size varies with temperature. The final calibration of the dam gives a Young's modulus of the masonry equal to 4000 MPa and a thermal coefficient of expansion equal to 1,2E-5 1/K.

which means, an 170% increase in the Young's modulus of the masonry and a 70% increase in the thermal coefficient of expansion, compared to the initial state, causes M3 to converge towards the target value (3,98E-4 m). The values of M1 and M2 converge in the best case, respectively, towards differences of 11,5% and 6% with the target values (1,06E-4 m and 2,44E-4 m).

- Comparison of the calibrations

As mentioned in the "calibration with static stress" section, the contribution of the 3D effect (not taken into account in this model) would have the effect of reinforcing the upper part of the dam and therefore of better approximating the IN-SITU deformations. So, the calibration of the 2D model can't be based on the static load. Thermal calibration is much more promising, with better convergence of relative displacements and more realistic material properties. These results are therefore retained for the 2D model.

In order to better understand the contribution of the 3D effect on the model, the first stones of a 3D digital model are laid in the appendix. Due to lack of time, this model could not be analyzed, but will be used in future studies of the Janov dam.

REFERENCES

Richtr, D., & Svejkovský, J. (n.d.). *VD JANOV -Rekonstrukce*, article. Retrieved Dam Days 2014, from http://www.emvizig.hu/Nemzetkozi/4_12_Svejkovsky_Richtr.pdf

Klármanová, B. *Janovská přehrada aneb kamenná krása*, bachelor thesis. Retrieved May 2, 2023, from

https://dspace.vsb.cz/bitstream/handle/10084/108279/KLA0031_HGF_B2110_2101R004_10_2014.pdf

Přehrady Povodí Ohře, Book. Retrieved Septembre 24, 2015, from https://web.archive.org/web/20150924075049/http://www.poh.cz/vd/vd_publikace/Povodi_Ohre_Vodni_dila_2010_cz.pdf

Časopis ZAKLÁDÁNÍ STAVEB, Magazine. Retrieved March, 2009, from https://www.zakladani.cz/casopis/pdf/ZS_04_2009.pdf

Údolní přehrada královského města Most v Čechách, article. Retrieved May 2, 2023, from https://www.poh.cz/StaticFiles//vd/files/janov/Janov_1911-14.pdf

Jan Vojtěchovský, Dalibor Louda. *Provozní řád pro vodní dílo Janov*, instruction manual. Retrieved October 16, 2018.

Goldgruber, Markus & Zenz, Gerald & Golger, Thomas. Analysis of Structural Safety of Gravity Dams, Article. January, 2012, from

https://www.researchgate.net/publication/304656777_Analysis_of_Structural_Safety_of_Gravity_Dams

Maltidis, Georgios & Stempniewski, Lothar & Fleischer, Helmut. The influence of post-tensioned anchors to the seismic behaviour of an old masonry gravity dam, Article. 28 August, 2013, from

https://henry.baw.de/server/api/core/bitstreams/20f5bce4-3597-4e18-a9b3-f435f79194e9/content

Jonas, Enzel & Markus Tollsten. Thermal cracking of a concrete arch dam due to seasonal temperature variations, Master thesis. August, 2017, from

https://kth.diva-portal.org/smash/get/diva2:1114901/FULLTEXT01.pdf

Rampal, Ajay & Halder, Prasun & Manna, Bappaditya & Sharma, Kapila. Static and Coupled Hydro-mechanical Analyses of Concrete Gravity Dam Resting on Jointed Rock Foundation, Article. 2020, from

https://www.researchgate.net/publication/340085755_Static_and_Coupled_Hydro-mechanical_Analyses_of_Concrete_Gravity_Dam_Resting_on_Jointed_Rock_Foundation/citation/download

Josef, Vorel & Miroslav, Kolařík & Boleslav, Březina. Report on the engineering geological survey of the site near the water of the Janov waterworks, Technical report. 2015.

Anton, J. Schleiss & Henri Pougatsch. LES BARRAGES Du projet à la mise en service, volume 17, Traité de Génie Civil. 2011.

V. Bettzieche & C. Heitefuss. Monitoring as a basis of cost-effective rehabilitation of an old masonry dam, Article. From

http://stauanlage.de/assets/applets/monitoringrehabilitation.pdf

I. Movilă & G. M. Atanasiu. Modelling of the Lateral Load behavior of Unreinforced Masonry Walls using the software Atena 2D, Article. 2012, from

https://www.iitk.ac.in/nicee/wcee/article/WCEE2012_1145.pdf

Manzini, Carlo Filippo & Magenes, Guido & Penna, Andrea & da porto, Francesca & Camilletti, Daniela & Cattari, Serena & Lagomarsino, Sergio. Masonry Italian Code-Conforming Buildings. Part 1: Case Studies and Design Methods, Journal of Earthquake Engineering. 2018, from:

https://www.researchgate.net/publication/329906799_Masonry_Italian_Code-Conforming_Buildings_Part_1_Case_Studies_and_Design_Methods

ANNEX – 3D MODEL

GEOMETRY AND MATERIAL PROPRIETIES

The figure 7.1 presents the 2 parts designed in the model, all defined as solid. The dam body is modeled as a monolithic block made of a single material, rubble masonry. The thickness of ashlar covering the dam is neglected for reasons of geometric simplification. The dam geometry is based on the technical report, for this study a longitudinal profile of the dam was drawn. In addition, several sensors were placed along 11 sections of the dam, including section 8v8n previously presented in the 2D model. Cutting out the dam geometry between these 2D sections will be decisive for the calibration part.

The highest part of the dam takes on the attributes of section 5L, previously presented for the 2D model, with a height Hf equal to the reservoir water level on the upstream side of the ham dam of 52.3 m, a base width b of 47.7 m and a crest width dc of 5.8 m. The shapes of the upstream and downstream faces are linear approximations of the arcs of circles R1 and R2, of radii 116 m and 226 m respectively. Using this section as a reference, an extrusion following the crown curve was made with a radius of 250 m and an arc length of 232 m. The longitudinal height of the dam is based on the longitudinal profile attributes presented in the technical report.

The dam rests on a broad base of bedrock, so dimensioned as to approximate as closely as possible the behaviour of the semi-infinite medium constituted by the foundation. The interface between the dam and the rock exactly matches the dam foundation based on the longitudinal profile presented in the technical report.

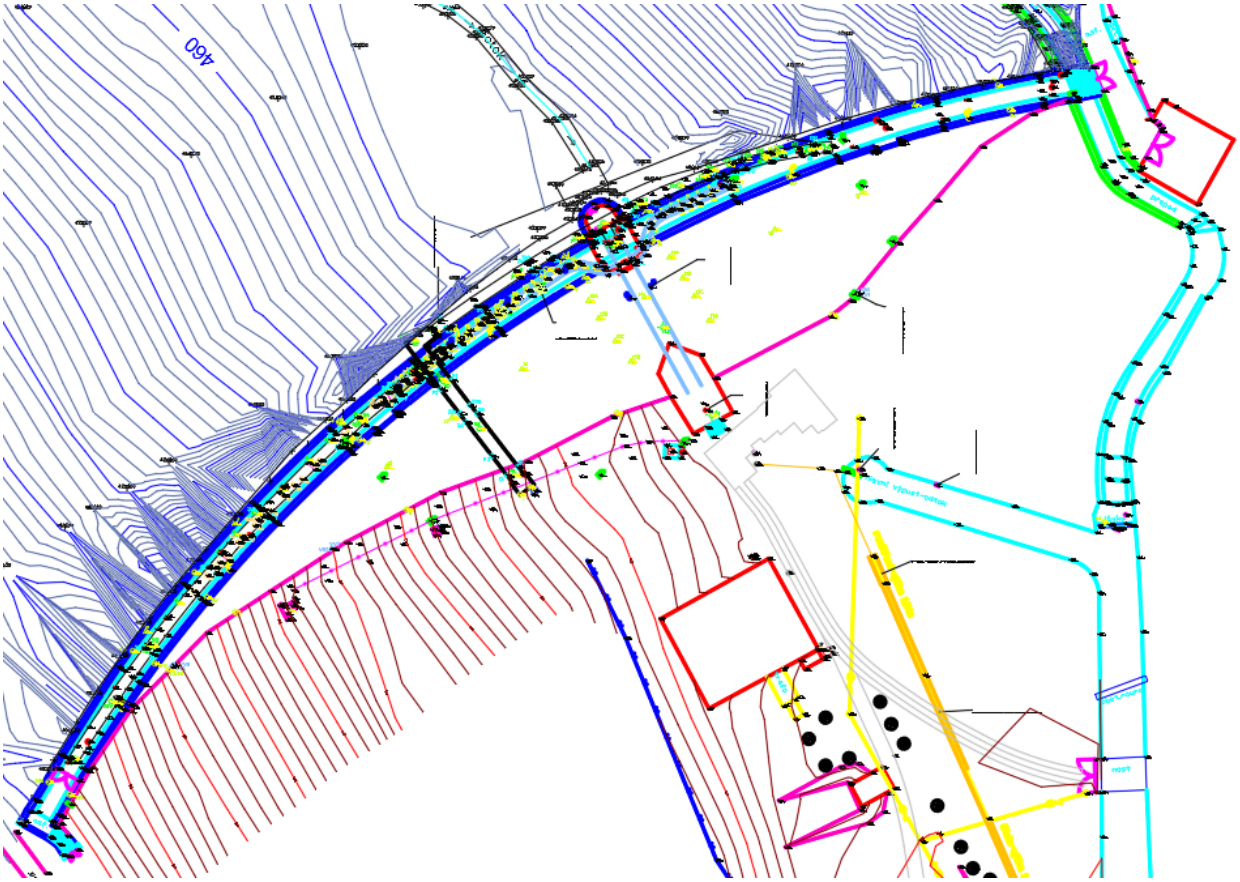

Figure 7.1 – Top view of Janov dam, © Technical report.

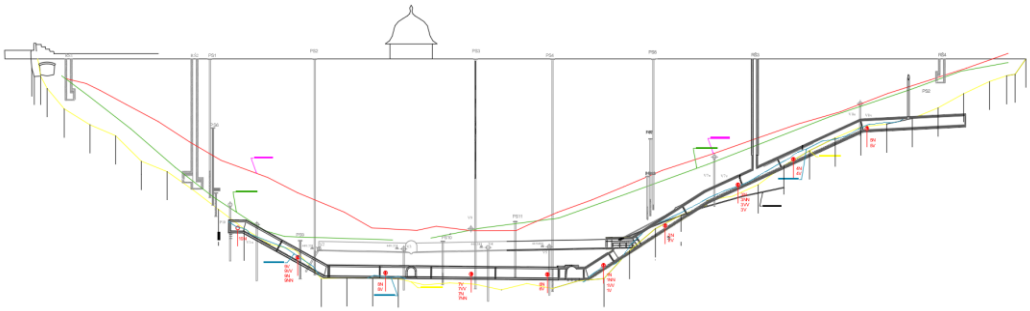

Figure 7.2 – Longitudinal view of the dam, © Technical report.

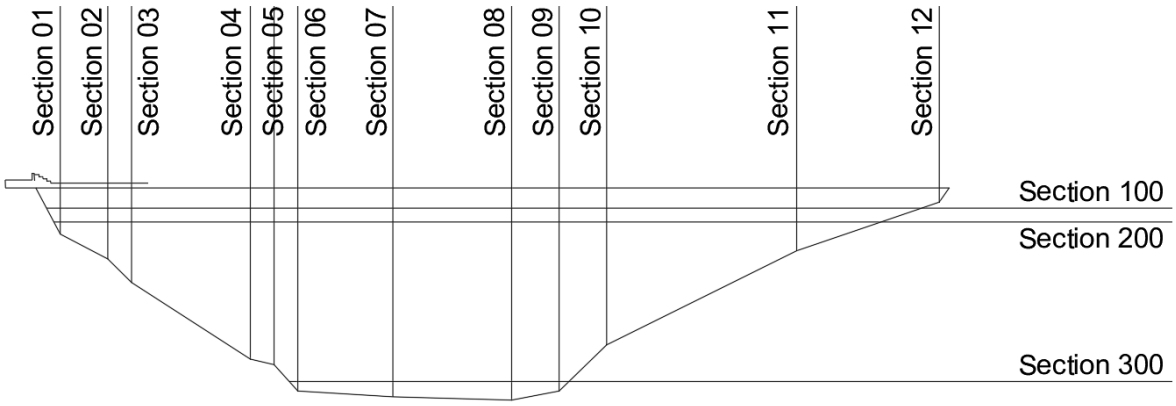

Figure 7.3 - Geometry of the analyzed arch dam based on the longitudinal view.

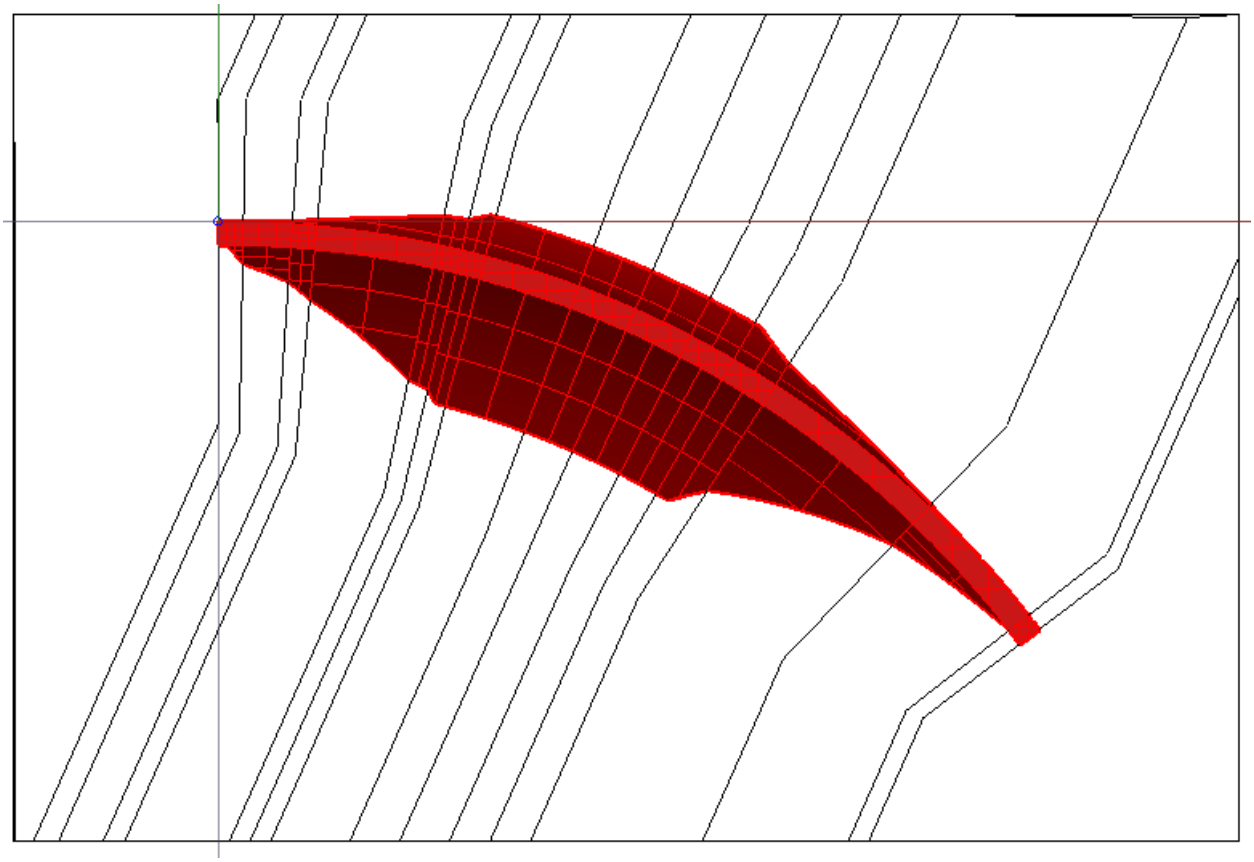

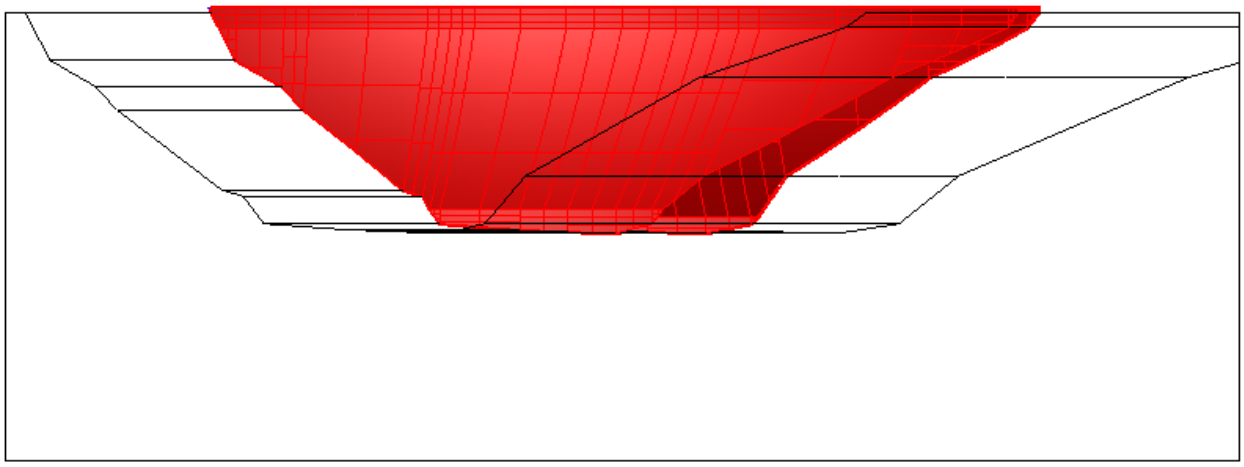

Figure 7.4 – View of the AutoCAD model of the dam and of the foundation (a) top view (b) profile view

The properties of the dam body elements and the rock mass on which it rests are presented, respectively, in Tables 7.1 and 7.2.

For masonry, the values of linear properties such as density ρ and Poisson's ratio α are based on the assumptions made in part 4.3 (Material proprieties) and the value of the Young's modulus is based on the thermic calibration of the 2D model. In the case of the rock mass, the properties are taken from the technical report carried out on the rock mass of the Janov dam in 2010-2015.

Young's modulus; E [Mpa]	Poisson's ratio; ν	Density; ρ [MN/m3]
1500	0,25	2,60E-02

Table 7.1 – Elastic proprieties of the masonry of the dam.

Young's modulus; E [Mpa]	Poisson's ratio; ν	Density; ρ [MN/m3]
4000	0,26	2.60E-02

Table 7.2 – Elastic proprieties of the rock foundation.

MESH

In the model, linear, tetrahedral elements were used for the masonry and rock. The elements along the interface between the arch and the foundation were fitted exactly to each other to ensure better contact for the irregular surface. The meshes are presented Figure 5.5.

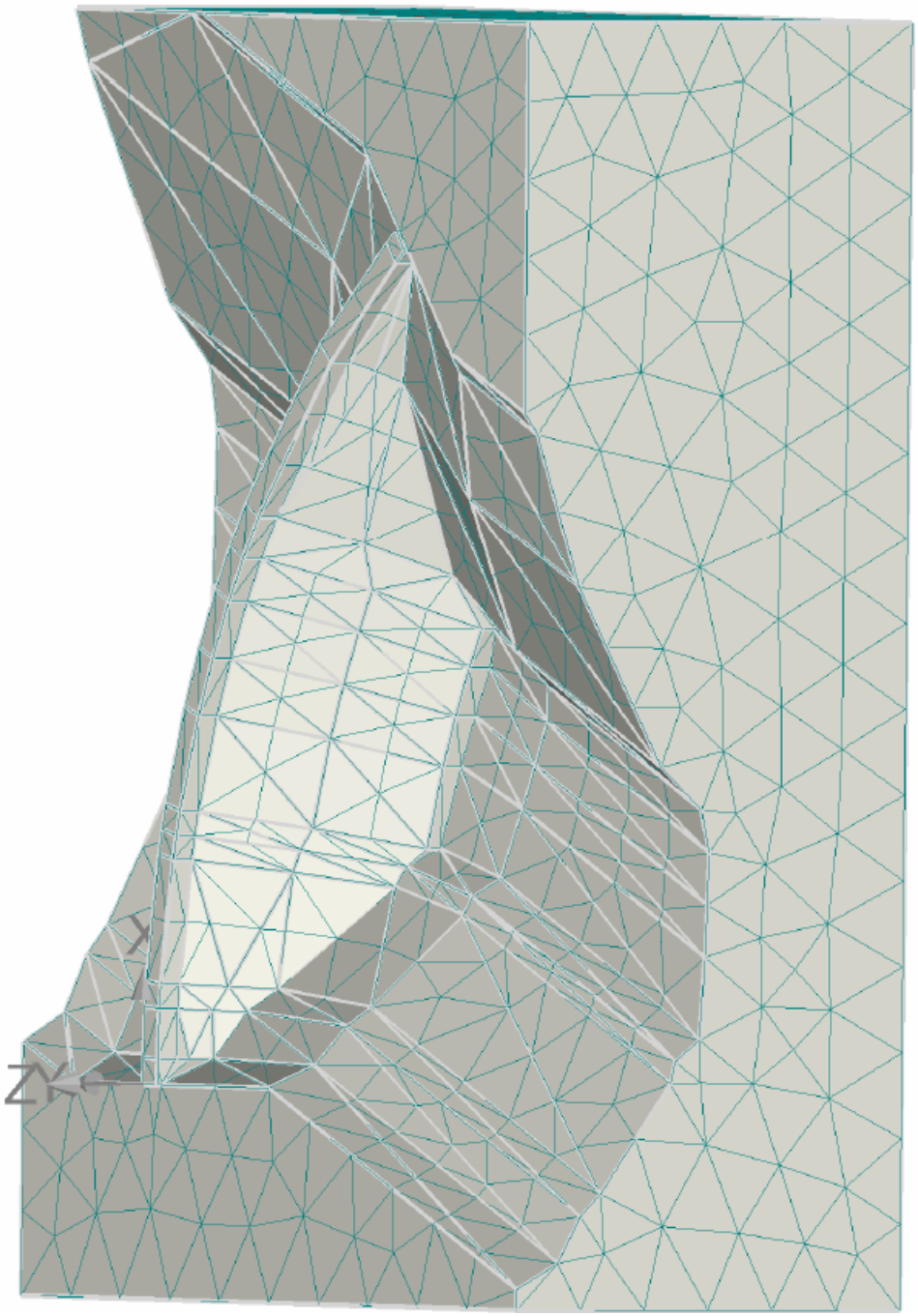

Figure 7.5 - Mesh in model 1

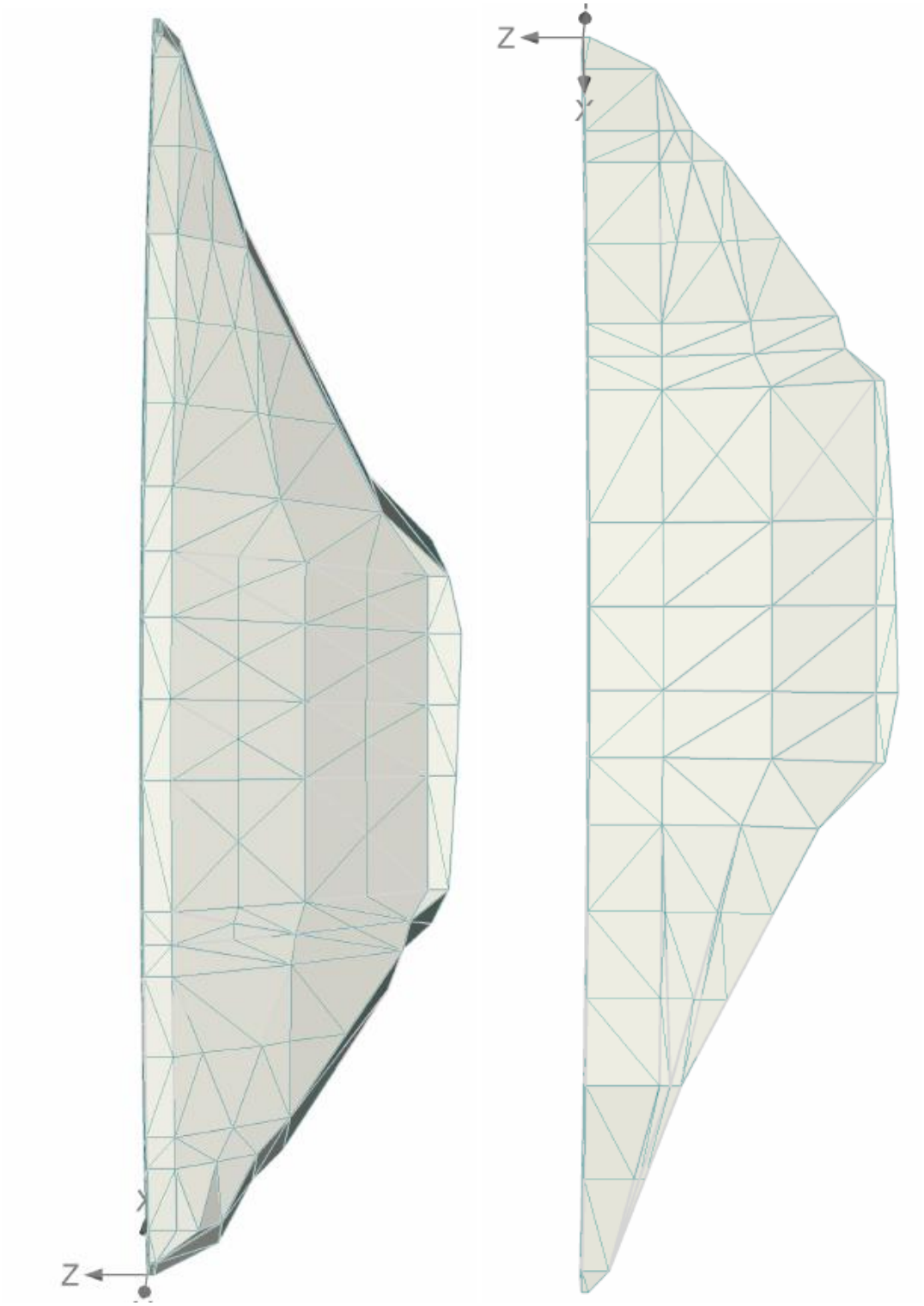

Figure 7.6 - Mesh of the dam in the (a) downstream face (b) upstream face.